ETGL-DDPG: A Deep Deterministic Policy Gradient Algorithm for Sparse Reward Continuous Control

Anonymous authors
Paper under double-blind review

Abstract

We consider deep deterministic policy gradient (DDPG) in the context of reinforcement learning with sparse rewards. To enhance exploration, we introduce a search procedure, ϵt-*greedy*, which generates exploratory options for exploring less-visited states. We prove that search using ϵt-greedy has polynomial sample complexity under mild MDP assumptions. To more efficiently use the information provided by rewarded transitions, we develop a new dual experience replay buffer framework, *GDRB*, and implement *longest n-step returns*. The resulting algorithm, *ETGL-DDPG*, integrates all three techniques: $\boldsymbol{\epsilon t}$-greedy, **G**DRB, and **L**ongest n-step, into DDPG. We evaluate ETGL-DDPG on standard benchmarks and demonstrate that it outperforms DDPG, as well as other state-of-the-art methods, across all tested sparse-reward continuous environments. Ablation studies further highlight how each strategy individually enhances the performance of DDPG in this setting.

1 Introduction

Deep deterministic policy gradient (DDPG) (Lillicrap et al., 2015) is one of the representative algorithms for reinforcement learning (RL) (Sutton & Barto, 2018), alongside other prominent approaches (Haarnoja et al., 2018; Fujimoto et al., 2018; Andrychowicz et al., 2017). In recent years, DDPG has served as the backbone algorithm for introducing novel ideas in robotics and RL Barth-Maron et al. (2018); Pan et al. (2020); Liu et al. (2023); Wang et al. (2023); Tiapkin et al. (2024). While DDPG demonstrates strong performance in continuous control tasks with dense reward signals (Duan et al., 2016; Kiran et al., 2021), its effectiveness diminishes significantly in sparse-reward settings where rewards are only observed upon reaching the goal (Matheron et al., 2019; Luck et al., 2019).

In sparse-reward environments where success depends on reaching a goal state, DDPG's deficiency can be explained from three perspectives. The first one is its lack of *directional exploration*. Like other off-policy RL algorithms, DDPG employs a *behavior policy* for exploring the environment. The standard choices are either an ϵ-greedy behavior policy that samples a random action with probability ϵ (e.g., 0.1), or the main policy with artificial noise. As argued in (Dabney et al., 2020), these one-step *noise augmented greedy* strategies are ineffective for exploring large sparse-reward state spaces due to the lack of temporal abstraction. To improve ϵ-greedy, Dabney et al. (2020) propose a temporally extended ϵz-greedy policy that expands exploration into multiple steps, controlled by a distribution z. ϵz-greedy represents an advancement from the option framework for reinforcement learning (Sutton et al., 1999). Theoretically, an option O is defined as a tuple $O = \langle I, \pi, \beta \rangle$, where I is the set of states where an option can begin, π is the option policy that determines which actions to take while executing the option, and β is the termination condition. In ϵz-greedy, each option repeats a primitive action for a specific number of time steps which is sampled from a distribution z (e.g., a uniform distribution). The option can begin at any state with probability ϵ and terminates whenever their length reaches a limit that is decided by z. While ϵz-greedy improves over ϵ-greedy, it is also *directionless*: for exploratory action, the agent does not use any information from its experience for more informed exploration.

The second drawback of DDPG is its uniform treatment of zero and non-zero rewards in the replay buffer. For most off-policy RL algorithms, a replay buffer is used to store and sample transitions of the agent's

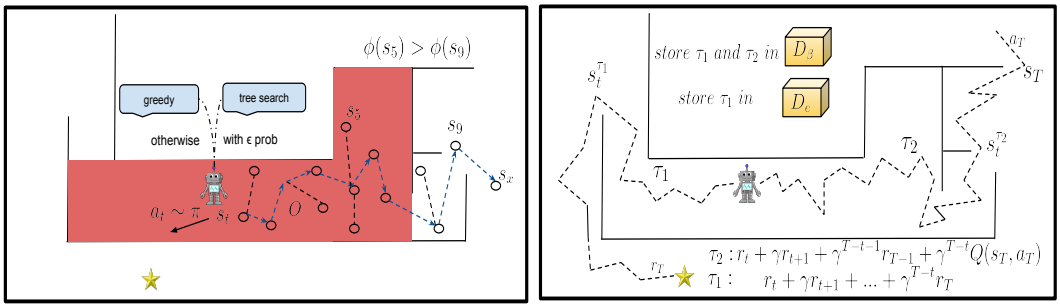

(a) ϵt-greedy: greedy or tree search

(b) GDRB and the longest n-step return

Figure 1: (a): ϵt-greedy exploration strategy. The agent creates a tree from the current state s_t with ϵ probability. Otherwise, it uses its policy to determine the next action $a_t \sim \pi$. The tree uses a hash function ϕ to estimate the visit counts to states. If the newly added node s_x to the tree is located in an unvisited area $n(\phi(s_x)) = 0$, the path from the root to that node is returned as option O. The tree helps in avoiding obstacles, discovering unexplored areas, and staying away from highly-visited regions (middle red area). (b): GDRB and the longest n-step return for Q-value updates. τ_1 reaches the goal (a successful episode), and τ_2 is truncated by time limit (an unsuccessful episode). The first buffer D_β stores both trajectories but D_e only stores successful trajectories. The target Q-value for state s_t is shown for both trajectories below the figure. In successful episodes, the target Q-value is the episode return. s_T represents the last state in each episode, which is the goal state indicated by a star in τ_1.

interactions with the environment. By default, DDPG uses a uniform sampling strategy that assigns an equal probability of being chosen to all transitions in the buffer. In sparse-reward environments, uniform sampling therefore rarely chooses rewarded transitions. In general, RL algorithms can be improved by prioritizing transitions based on the associated rewards or TD error (Schaul et al., 2015). For problems with well-defined goals, a replay buffer can be further enhanced to exploit the strong correlation of rewards and goals. The third weakness of DDPG is its slow information propagation when updating its learning policy. Since only the last transition in a successful episode (i.e., goal reached) gets rewarded, in standard DDPG, the agent must achieve the goal many times to make sure that the reward is eventually propagated backward to early states. It is known that one way to achieve this is to provide intermediate rewards with reward shaping methods (Laud, 2004). However, effective reward shaping is usually problem-specific and does not generalize to a wide range of tasks.

In this paper, we enhance DDPG (Lillicrap et al., 2015) to address all three aforementioned problems. Our first contribution is *ϵt-greedy*, a new temporally version of ϵ-greedy that utilizes a light-weight search procedure, similar to Laud (2004), to enable more directional exploration based on the agent's previous experience data. We show that similar to ϵz-greedy, ϵt-greedy has polynomial sample complexity in related parameters of the MDP. Our second contribution is a new *goal-conditioned dual replay buffer* (GDRB), that uses two replay buffers along with an adaptive sampling strategy to differentiate goal-reached and goal-not-reached experience data. These two buffers differ in retention policy, size, and the transitions they store. Our third enhancement is to replace the one-step update in DDPG with the *longest n-step return* for all transitions in an episode. Figure 1 illustrates the innovations of ETGL-DDPG. In Section 4, we evaluate the performance of ETGL-DDPG through extensive experiments on 2D and 3D continuous control benchmarks. As the proposed strategies are orthogonal, we show that each of the three strategies individually improves the performance of DDPG via a thorough ablation study. Furthermore, ETGL-DDPG outperforms current state-of-the-art methods across all tested environments.

2 Background

We consider a Markov decision process (MDP) defined by the tuple $(S, A, \mathcal{T}, r, \gamma, \rho)$. S is the set of states, A is the set of actions, $\mathcal{T}(s'|s, a)$ is the transition distribution, $r : S \times A \times S \to \mathbb{R}$ is the reward function, $\gamma \in [0, 1]$ is the discount factor, and $\rho(s_0, s_g)$ is the distribution from which initial and goal states are sampled for each

episode. Every episode starts with sampling a new pair of initial and goal states. At each time-step t, the agent chooses an action using its policy and considering the current state and the goal state $a_t = \pi(s_t, s_g)$ resulting in reward $r_t = (s_t, a_t, s_g)$. The next state is sampled from $\mathcal{T}(.|s_t, a_t)$. The episode ends when either the goal state or the maximum number of steps T is reached. The return is the discounted sum of future rewards $R_t = \sum_{i=t}^{T} \gamma^{i-t} r_i$. The Q-function and value function associated with the agent's policy are defined as $Q^\pi(s_t, a_t, s_g) = \mathbb{E}[R_t|s_t, a_t, s_g]$ and $V^\pi(s_t, s_g) = max_a Q^\pi(s_t, a_t, s_g)$. The agent's objective is to learn an optimal policy π^* that maximizes the expected return $\mathbb{E}_{s_0}[R_0|s_0, s_g]$.

2.1 Deep Deterministic Policy Gradient (DDPG)

To ease presentation, we adopt our notation with explicit reference to the goal state for both the critic and the actor networks in DDPG. DDPG maintains an actor $\mu(s, s_g)$ and a critic $Q(s, a, s_g)$. The agent explores the environment through a stochastic policy $a \sim \mu(s, s_g) + w$, where w is a noise sampled from a normal distribution or an Ornstein-Uhlenbeck process (Uhlenbeck & Ornstein, 1930). To update both actor and critic, transition tuples are sampled from a replay buffer to perform a mini-batch gradient descent. The critic is updated by a loss L,

$$L = \mathbb{E}[Q(s_t, a_t, s_g) - y_t]^2 \tag{1}$$

where $y_t = r_t + \gamma Q'(s_{t+1}, \mu'(s_{t+1}, s_g), s_g)$. Q' and μ' are the target critic and actor, respectively; their weights are soft-updated to the current weights of the main critic and actor, respectively. The actor is updated by the deterministic policy gradient algorithm (Silver et al., 2014) to maximize the estimated Q-values of the critic using loss $-\mathbb{E}_s[Q(s, \mu(s, s_g), s_g)]$.

2.2 Locality-Sensitive Hashing

Our approach discretizes the state space with a hash function $\phi : \mathbb{S} \to \mathbb{M}$, that maps states to buckets in $\mathbb{M}$. When we encounter a state s, we increment the visit count for $\phi(s)$. We use $n(\phi(s))$ as the visit counts of all states that map to the same bucket $\phi(s)$. Clearly, the *granularity* of the discretization significantly impacts our exploration method. The goal for the granularity is that "distant" states are in separate buckets while "similar" states are grouped into one.

We use Locality-Sensitive Hashing (LSH) as our hashing function, a popular class of hash functions for querying nearest neighbors based on a similarity metric (Bloom, 1970). SimHash (Charikar, 2002) is a computationally efficient LSH method that calculates similarity based on angular distance. SimHash retrieves a binary code of state $s \in S$ as

$$\phi(s) = sgn(Af(s)) \in \{-1, 1\}^k, \tag{2}$$

where $f : S \to \mathbb{R}^D$ is a preprocessing function and A is a $k \times D$ matrix with i.i.d. entries drawn from a standard Gaussian distribution $\mathcal{N}(0, 1)$. The parameter k determines the granularity of the hash: larger values result in fewer collisions, thereby enhancing the ability to distinguish between different states.

3 The ETGL-DDPG Method

In this section, we describe three strategies in ETGL-DDPG for improving DDPG in sparse-reward tasks. The full pseudocode for ETGL-DDPG is presented in Supplementary Algorithm 3.

3.1 ϵt-Greedy: Exploration With Search

In principle, exploration should be highest at the beginning of training, as discovering rewarded transitions during early steps is essential for escaping local optima (Matheron et al., 2019). Motivated by the success of the fast exploration algorithms RRT (LaValle, 1998) and ϵz-greedy (Dabney et al., 2020), we introduce

ϵt-greedy, which combines ϵ-greedy with a *tree search* procedure. Like ϵ-greedy, ϵt-greedy selects a greedy action with probability $1-\epsilon$, and an exploratory action with probability ϵ. However, instead of exploring uniformly at random, the exploratory action in ϵt-greedy is the first step of an *option* generated via a search with time budget N.

To execute the search process, the agent requires access to the environment's transition function $\mathcal{T}$ of the corresponding MDP. This is used to generate new nodes within the search tree. However, since our exploration strategy is built on DDPG, the model-free algorithm, the transition function $\mathcal{T}$ is not known. Instead, the agent utilizes its replay buffer to advance the search. We briefly discuss the impact of having access to $\mathcal{T}$ on the exploration process in Supplementary Material A.4. We also assume that the agent has a SimHash function ϕ, which discretizes the large continuous environment. For each state s, $n(\phi(s))$ serves as an estimate of the number of visits to a neighbourhood of s throughout the entire learning process.

The replay buffer contains transitions observed during training. It can be used as a transition model for observed transitions and an approximate one for transitions similar to those already seen. For simplicity, we identify each bucket with its hash code $\phi(s)$. We use a buffer B_M which stores observed transitions based on the hash of their states $\phi(s)$. If the agent makes a transition (s_t, a_t, r_t, s_{t+1}) in the environment, the transition is stored in bucket $b = \phi(s_t)$. All transitions are assigned to their buckets upon being added to the replay buffer. As training may take a long time, we limit the number of transitions in each bucket, and randomly replace one of the old transitions in a full bucket with the new transition.

The function `next_state_from_replay_buffer` in Algorithm 1 shows how new nodes can be added to the search: assuming we are at node s_x, we randomly select a transition (s', a, r, s'') in bucket $\phi(s_x)$ and create a new child $s_{x'}$ for s_x by using following approximation:

$$\mathcal{T}(s_x, a) \approx \mathcal{T}(s', a) \tag{3}$$

Algorithm 1 explains how the search generates an exploratory option. Initially, at state s, we create a list of frontier nodes consisting of only the root node s. If bucket of state s in B_M is empty: $b_{\phi(s)} = \varnothing$, there is no transition to approximate $\mathcal{T}(s, a)$. In this case, ϵt-greedy as in ϵ-greedy generates a random action at s. Otherwise, when $b_{\phi(s)} \neq \varnothing$, ϵt-greedy conducts a tree search iteratively, with a maximum of N iterations. At each iteration, a node s_x is sampled uniformly from the frontier nodes, and a *child* for s_x, noted as $s_{x'}$, is generated using `next_state_from_replay_buffer` function. If $n(\phi(s_{x'})) = 0$, we terminate and return the action sequence from the root to $s_{x'}$; otherwise, we repeat this process until we have added N nodes to the tree. We then return the action sequence from the root to a least-visited node s_{min}:

$$s_{min} = \min_{s \,\in\, frontier\ nodes} n(\phi(s)) \tag{4}$$

To justify this exploration method, we adopt the conditions outlined in Liu & Brunskill (2018) to validate the sample efficiency of ϵt-greedy. We begin by introducing the relevant terms and then present the main theorem. Detailed definitions and proofs are provided in Appendix A.1. The key idea is to define a measure that captures the concept of visiting all state-action pairs, as outlined in Definition 1.

Definition 1 (**Covering Length**). *The covering length (Even-Dar & Mansour, 2004) represents the minimum number of steps an agent must take in an MDP, starting from any state-action pair $(s, a) \in \mathcal{S} \times \mathcal{A}$, to visit all state-action pairs at least once with a probability of at least 0.5.*

Our objective is to find a near-optimal policy, as defined in Definition 2.

Definition 2 (**ϵ-optimal Policy**). *A policy π is called ϵ-optimal if it satisfies $V^{\pi^*}(s) - V^{\pi}(s) \leq \epsilon$, for all $s \in S$, where $\epsilon > 0$.*

Next, we define the concept of sample efficiency, which is captured through the notion of polynomial sample complexity in Definition 3.

Definition 3 (**PAC-MDP Algorithm**). *Given a state space $\mathcal{S}$, action space $\mathcal{A}$, suboptimality error $\epsilon > 0$ (from Definition 2) and $0 < \delta < 1$, an algorithm $\mathcal{A}$ is called PAC-MDP (Kakade, 2003), if the number*

of time steps required to find a ϵ-optimal policy is less than some polynomial in the relevant quantities $(|\mathcal{S}|, |\mathcal{A}|, \frac{1}{\epsilon}, \frac{1}{1-\gamma}, \frac{1}{\delta})$ *with probability at least* $1-\delta$.

For simplicity, when we say an algorithm $\mathcal{A}$ has polynomial sample complexity, we imply that $\mathcal{A}$ is PAC-MDP. The work by Liu & Brunskill (2018) establishes polynomial sample complexity for a uniformly random exploration by bounding the covering length defined in Definition 1. Using this, and considering a limited tree budget N, we show that ϵt-greedy is PAC-MDP. Let's denote the search tree by $\mathcal{X}$, and the distribution over the generated options in $\mathcal{X}$ as $\mathcal{P}_{\mathcal{X}}$. The following Theorem provides a lower bound on option sampling in tree $\mathcal{X}$ under certain condition.

Theorem 1 (**Worst-Case Sampling**). *Given a tree $\mathcal{X}$ with N nodes (s_1 to s_N), for any $\omega \in \Omega_{\mathcal{X}}$, the sampling probability satisfies:*

$$\mathcal{P}_{\mathcal{X}}[\omega] \geq \frac{1}{N!(\max_{i\in[N]} |\phi(s_i)|)^{N-1}} \geq \frac{1}{\Theta(|\mathcal{S}||\mathcal{A}|)} \tag{5}$$

*, **if** $N \leq \frac{\log(|\mathcal{S}||\mathcal{A}|)}{\log\log(|\mathcal{S}||\mathcal{A}|)}$. Here, $\mathcal{S}$ and $\mathcal{A}$ represent the state space and action space, respectively.*

To prove Theorem 1, we examine the construction of the "hardest option", $\hat{\omega} \in \Omega_{\mathcal{X}}$, which has the lowest sampling probability in the tree $\mathcal{X}$. Since $\mathcal{P}_{\mathcal{X}}$ is an unknown distribution, we cannot directly exploit it. Instead, we construct a worst-case scenario to approximate the minimum option sampling probability. Now, we present the following Theorem on the sample complexity of ϵt-greedy.

Theorem 2 (**ϵt-greedy Sample Efficiency**). *Given a state space $\mathcal{S}$, action space $\mathcal{A}$, and a set of options $\Omega_{\mathcal{X}}$ generated by ϵt-greedy for each tree $\mathcal{X}$, if $\mathcal{P}_{\mathcal{X}}[\omega] \geq \frac{1}{\Theta(|\mathcal{S}||\mathcal{A}|)}$, ϵt-greedy achieves polynomial sample complexity or i.e. is PAC-MDP.*

Theorem 1 asserts that the sampling bound condition from Theorem 2 is satisfied when $N \leq \frac{\log(|\mathcal{S}||\mathcal{A}|)}{\log\log(|\mathcal{S}||\mathcal{A}|)}$. Theorem 2 establishes the necessary lower bound on the sampling probability of an option $\omega \in \Omega_{\mathcal{X}}$ for any given exploration tree $\mathcal{X}$, ensuring that the ϵt-greedy strategy is PAC-MDP under this criterion.

3.2 GDRB: Goal-conditioned Dual Replay Buffer

The experience replay buffer is an indispensable part of deep off-policy RL algorithms. It is common to use only one buffer to store all transitions and use FIFO as the retention policy, with the most recent data replacing the oldest data (Mnih et al., 2013). As an alternative, in the reservoir sampling (Vitter, 1985) retention policy, each transition in the buffer has an equal chance of being overwritten. This maintains coverage of some older data over training. *RS-DRB* (Zhang et al., 2019) uses two replay buffers, one for exploitation and the other for exploration. The transitions made by the agent's policy are stored in the exploitation buffer, and the random exploratory transitions are stored in the exploration buffer. For the retention policy, the exploration buffer uses reservoir sampling, while the exploitation buffer uses FIFO.

Inspired by this dual replay buffer framework, we propose a *Goal-conditioned Double Replay Buffer (GDRB)*. The first buffer D_β stores all transitions during training, and the second buffer D_e stores the transitions that belong to successful episodes (i.e., goal reached). D_β uses reservoir sampling, and D_e uses FIFO. Since D_β needs to cover transitions from the entire training process, it is larger than D_e. We balance the number of samples taken from the two buffers with an adaptive sampling ratio. Specifically, in a training process of E episodes, at current episode i, the sampling ratios τ_e and τ_β for D_e and D_β are set as follows: $\tau_e = \frac{i}{E}, \tau_\beta = 1 - \tau_e$. To select C mini-batches, $\max(\lfloor \tau_\beta * C \rfloor, 1)$ mini-batches are chosen from D_β and the rest from D_e. Later stages of training still sample from D_β to not forget previously acquired knowledge, as we assume the policy is more likely to reach the goal as the training progresses. In case that D_e is empty, since there are no successful episodes yet, we draw all mini-batches from D_β.

3.3 Using Longest n-step Return

In standard DDPG, Q-values are updated using one-step TD. In goal-reaching tasks with sparse rewards, only one rewarded transition per successful episode is added to the replay buffer. The agent needs rewards

Algorithm 1 Generating exploratory option with tree search

```
function generate_option(state s, hash function φ, budget N)
    frontier_nodes ← {}
    Initialize root using s: root ← TreeNode(s)
    frontier_nodes ← frontier_nodes ∪ {root};
    s_min ← root
    i ← 0
    while i < N do
        s_x ∼ UniformRandom(frontier_nodes)
        s_x' = next_state_from_buffer(s_x)
        if n(φ(s_x'))=0 then
            Extract option o by actions root to s_x'
            return o
        end if
        if n(φ(s_x')) < n(φ(s_min)) then
            s_min=s_x'
        end if
        i ← i + 1
    end while
    Extract option o by actions root to s_min
    return o
end function

function next_state_from_buffer(s_x, frontier_nodes)
    (s', a, r, s'') ∼ UnifromRandom(φ(s_x))
    s_x' ← s''
    s_x.add_child(s_x')
    frontier_nodes ← frontier_nodes ∪ {s_x'}
    return s_x'
end function
```

provided by these transitions to update its policy toward reaching the goal. With few rewarded transitions, the agent should exploit a successful path to the goal many times so the reward is propagated backward quickly. Multi-step updates can accelerate this process by looking ahead several steps, resulting in more rewarded transitions in the replay buffer (Meng et al., 2021; Hessel et al., 2018). For example, Meng et al. (2021) utilize n-step updates in DDPG with n ranging from 1 to 8. In our design, to share the reward from the last step of a successful episode for all transitions in the episode, we use *longest n-step return* (Mnih et al., 2016), shown in Equation 6.

$$Q(s_t, a_t) = \begin{cases} \sum_{k=0}^{T-t} \gamma^k r_{t+k}, & s_T \text{ is a goal state} \\ \sum_{k=0}^{T-t-1} \gamma^k r_{t+k} + \gamma^{T-t} Q(s_T, a_T), & \text{otherwise} \end{cases} \tag{6}$$

Here, s_T is the last state in the episode. Using the longest n-step return for each transition from a successful episode, the reward is immediately propagated to all Q-value updates. In unsuccessful episodes, using the longest n-step return reduces the overestimation bias in Q-values (Thrun & Schwartz, 1993). Meng et al. (2021) empirically show that using multi-step updates can improve the performance of DDPG on robotic tasks mostly by reducing overestimation bias — they demonstrate that the larger the number of steps, the lower the estimated target Q-value and overestimation bias.

4 Experiments

In this section, we show the details of how ETGL-DDPG improves DDPG for sparse-reward tasks using its three strategies. We use experiments to answer the following questions: 1) Can ETGL-DDPG outperform state-of-the-art methods in goal-reaching tasks with sparse rewards? 2) How does each of these three in-

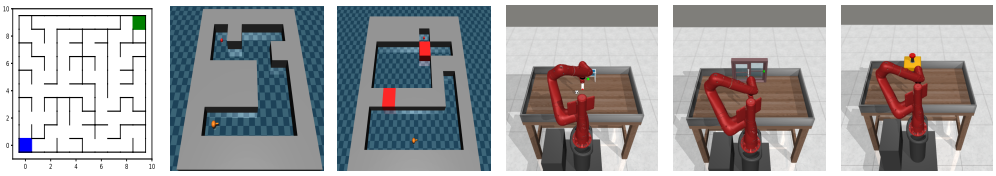

(a) Wall-maze (b) U-maze (c) Point-push (d) soccer (e) window-open (f) press-button

Figure 2: The environments used in our experiments.

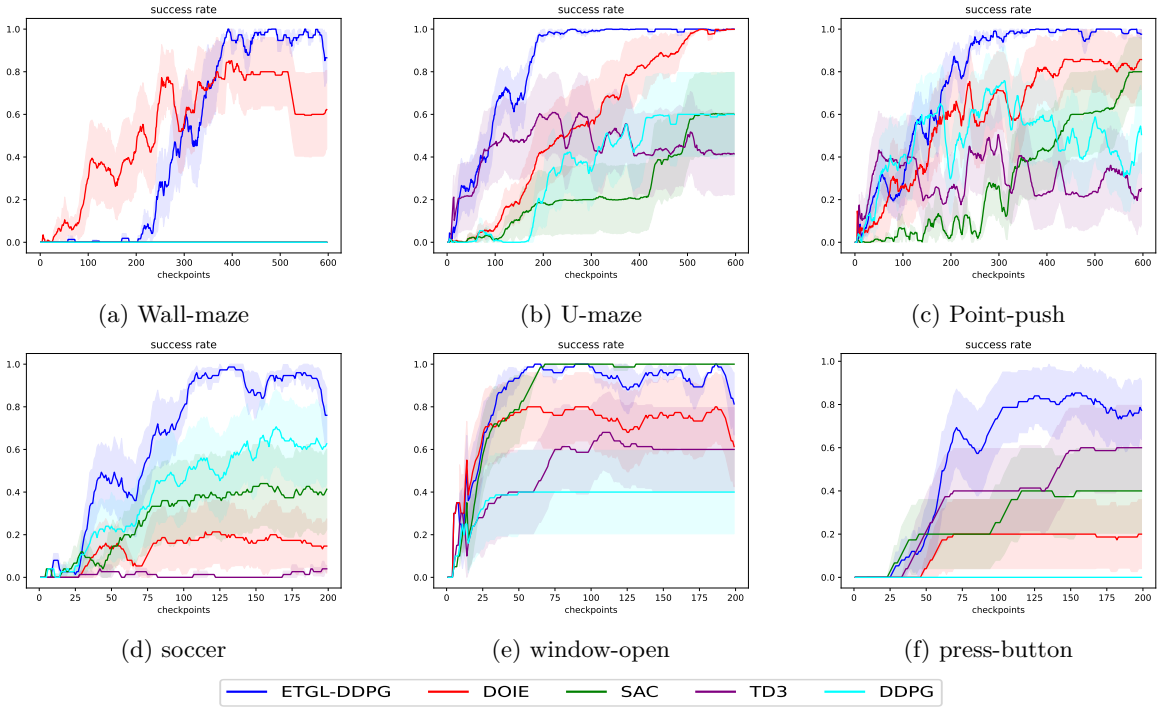

(a) Wall-maze (b) U-maze (c) Point-push

(d) soccer (e) window-open (f) press-button

Figure 3: The success rates across all environments, averaged over 5 runs with different random seeds. Shaded areas represent one standard deviation. We trained all methods for 6 million frames in the navigation environments and 2 million frames in the manipulation environments, with success rates reported at every 10^5-step checkpoint. A moving average with a window size of 10 is applied to all methods for better readability.

novations impact the performance of DDPG? 3) Can ϵt-greedy explore more efficiently than ϵz-greedy and other common exploration strategies?

We consider two types of tasks: *navigation* and *manipulation*. We use three sparse-reward continuous environments for navigation. The first environment is a 2D maze called *Wall-maze* (Trott et al., 2019), where a reward of -1 is given at each step, and a reward of 10 is given if the goal is reached. The start and goal states for each episode are randomly selected from the blue and green regions, respectively, as shown in Figure 2a. The agent's action (dx,dy) determines the amount of movement along both axes. The environment contains a gradient cliff feature (Lehman et al., 2018), where the fastest way to reach the goal results in a deadlock close to the goal. Our second and third 3D environments are *U-maze* (Figure 2b) and *Point-push* (Figure 2c) (Kanagawa, 2021), designed using the MuJoCo physics engine (Todorov et al., 2012). In both environments, a robot (orange ball) seeks to reach the goal (red region). In Point-push, the robot must additionally push aside the two movable red blocks that obstruct the path to the goal. A small negative reward of -0.001 is given at each step unless the goal is reached, where the reward is 1. In each episode, the robot starts near the same position with slight random variations, but the goal region remains fixed.

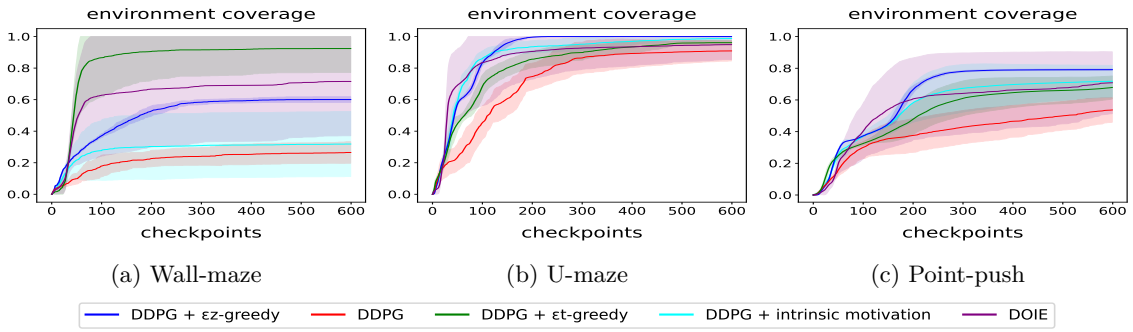

(a) Wall-maze (b) U-maze (c) Point-push

Figure 4: The environment coverage for exploration strategies in navigation environments. On the graph, the y-axis indicates the portion of the environment that has been covered, and the checkpoints occur every 10^4 steps shown on the x-axis. The results are given for the average of 10 runs with random seeds. The shaded region represents one standard deviation.

We also employ three manipulation tasks: *window-open*, *soccer*, and *button-press* (Figures 2d, e, and f) (Yu et al., 2020). In window-open, the goal is to push the window open; in soccer, the goal is to kick the ball into the goal; and in button-press, the aim is to press the top-down button. Each episode begins with the robot's gripper in a randomized starting position, while the positions of other objects remain constant. The original versions of these tasks employ a uniquely shaped reward function for each task. However, these versions offer limited challenges for exploration, as standard baselines, such as SAC, demonstrate strong performance (Yu et al., 2020). We modified the original reward function to be sparse, transforming these tasks into challenging exploration problems.

The maximum number of steps per episode is set to 100 for Wall-maze and 500 for all other environments. Across all methods, the neural network architecture consists of 3 hidden layers with 128 units each, using ReLU activation functions. For standard baselines, we utilize the implementations from OpenAI Gym (Dhariwal et al., 2017), and for other baselines, we rely on their publicly available implementations. After testing various configurations, we found that ϵt-greedy and ϵz-greedy perform best with budgets of $N = 40$ and $N = 15$, respectively, across these environments. Additional details about the environments and experimental setup are provided in Appendix A.5.

4.1 Overall Performance of ETGL-DDPG

We evaluate the performance of ETGL-DDPG compared to state-of-the-art methods. We compare with SAC (Haarnoja et al., 2018), TD3 (Fujimoto et al., 2018), DDPG, and DOIE (Lobel et al., 2022). DOIE demonstrates state-of-the-art performance in challenging sparse-reward continuous control problems by drastically improving the exploration. While both DOIE and ϵt-greedy use a similarity measure between new and observed states, DOIE applies this to compute an optimistic value function rather than solely guiding the agent to unexplored areas. The results are shown in Figure 3. In the navigation environments, ETGL-DDPG and DOIE demonstrate superior performance compared to other methods, with ETGL-DDPG achieving a success rate of 1 faster than DOIE. Notably, Wall-maze presents a more challenging task among navigation environments, where only ETGL-DDPG and DOIE are able to achieve a success rate above zero. In manipulation tasks, the press-button poses the hardest challenge as none of the methods achieve a success rate of 1. ETGL-DDPG still outperforms all other approaches, while DOIE underperforms compared to SAC, indicating its limitations in adapting to high dimensional environments.

4.2 Environment Coverage through Exploration

We now examine how effective ϵt-greedy is in covering the environment. To do so, we discretize the navigation environments into small cells. A cell is considered visited if the agent encounters a sufficient number of distinct states within it, and the overall environment coverage is quantified as the fraction of visited cells. Figure 4 presents a comparison of environment coverage across different exploration strategies. All strategies

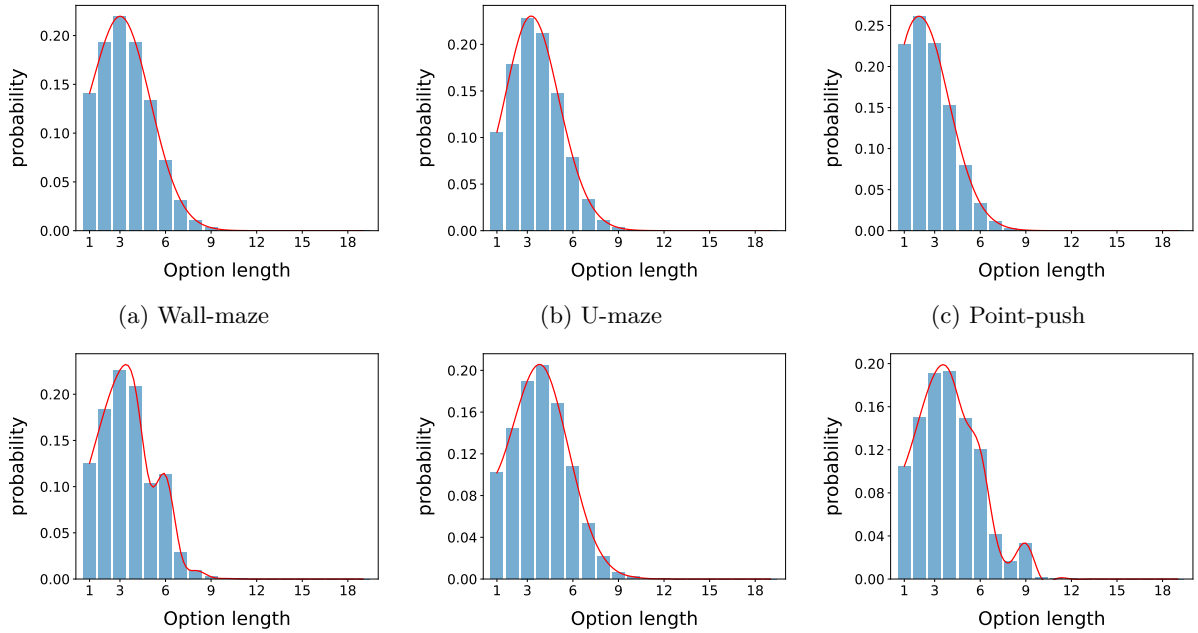

(a) Wall-maze (b) U-maze (c) Point-push

(d) soccer (e) window-open (f) press-button

Figure 5: The distribution of options chosen in training. The x-axis represents the length of the options and the y-axis indicates the probability of each length, calculated based on how often each length is chosen across all options.

except DOIE, which uses Radial Basis Function Deep Q-Network (RBFDQN) (Asadi et al., 2021), use DDPG as their underlying algorithm. RBFDQN is an enhanced DQN variant that incorporates Radial Basis Functions (RBF) to achieve more accurate Q-value approximations in continuous environments. In Wall-maze, ϵt-greedy achieves 80% coverage, whereas DOIE reaches 60%. ϵz-greedy covers approximately half of the environment, whereas the remaining methods manage to explore only around 30%. In U-maze, all strategies are successful, covering 80% or more of the environment. Even so, ϵz-greedy reaches full coverage faster than other methods. In Point-push, none of the methods can fully cover the environment and ultimately achieve nearly the same coverage. The tree budget N serves as an upper bound on the option length in ϵt-greedy, analogous to its role in ϵz-greedy when using a uniform distribution $z(n) = \mathbb{1}_{n \leq N}/N$. We evaluate environment coverage under varying values of N in Section A.7, where results indicate that ϵt-greedy achieves improved coverage as N increases. In contrast, ϵz-greedy does not exhibit a consistent improvement in coverage and, in some cases, experiences a decline. This highlights the advantages of directed exploration over undirected approaches. Finally, we present the distribution of final states reached in the episodes to illustrate the order in which the agent visits different regions of the environment (see Appendix A.8).

In ϵz-greedy, various distributions can be used to select options based on their length. Although a uniform distribution is a straightforward choice, alternative distributions such as the zeta distribution $z(n) \propto n^{-\mu}$ (where μ controls the decay rate) can also be employed. Empirical results by (Dabney et al., 2020) show that the zeta distribution slightly outperforms the uniform distribution, and moreover, produces a pattern akin to *Lévy flights* observed in certain ecological foraging models (Baronchelli & Radicchi, 2013). Figure 5 shows the distribution of option lengths generated by ϵt-greedy during training across all environments, revealing two main observations: (1) moderate-length options have the highest probability of being selected, and (2) probabilities decay as option length increases. While this decay pattern resembles that of the zeta distribution (where length 1 is most likely), ϵt-greedy instead favors moderate lengths. Note that Although options longer than 12 do occur, their frequency is extremely low and thus not visible in Figure 5.

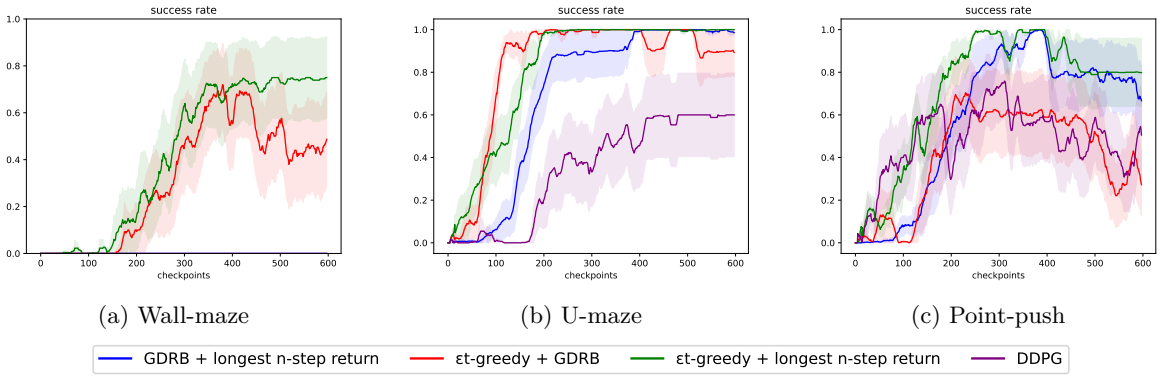

(a) Wall-maze (b) U-maze (c) Point-push

Figure 6: The ablation study for two-component combinations in navigation environments. The success rates are averaged over 5 runs with different random seeds and the shaded areas represent one standard deviation.

4.3 Effectiveness of Each New Component in ETGL-DDPG

We evaluated the performance of ETGL-DDPG, and now we assess the impact of each component on DDPG separately. Figure 7 presents the results for all environments. ϵt-greedy demonstrates the most improvement across all environments and is the only method that enhances the performance of DDPG in the Wall-maze, highlighting the critical role of our exploration strategy. GDRB shows a positive impact on DDPG performance in all environments, except for soccer, where DDPG alone outperforms all baselines. Additionally, we replaced reservoir sampling with FIFO as the retention policy in GDRB and observed similar results. The longest n-step return has a positive effect only in U-maze and press-button tasks, while it negatively impacts performance in soccer and Point-push. We attribute this to the inherently high variance of multi-step updates. A comparison of Figures 3 and 7 across all environments shows that ETGL-DDPG consistently outperforms the use of each component individually, supporting the effectiveness of their combination.

To conclude the analysis of each component, we conduct three additional experiments in this section. First, we perform an ablation study by considering all possible two-component combinations, where the omitted component in each combination is replaced with its DDPG counterpart. The results, shown in Figure 6 for the navigation environments, indicate that all combinations outperform DDPG in every environment except *Wall-maze*, where the agent fails to achieve a non-zero success rate without ϵ-greedy exploration. Moreover, in *Point-push*, omitting the longest n-step return while following the original DDPG strategy causes a noticeable decline in success rates during the later stages of training.

Second, we compare the longest n-step return with the method proposed by Meng et al. (2021), who experimented with n ranging from 1 to 8 and tested both the minimum of the n-step returns and their average. In their experiments, *MMDDPG*, which computes the average return over 1 to 8 steps (*avg8-step*), outperforms other variants in robotic tasks. Here, we replace the longest n-step return in ETGL-DDPG with the avg8-step return to evaluate its effectiveness in reward propagation. The results, presented in Appendix A.2, show that both methods perform similarly across most environments, except in *Wall-maze*, where the longest n-step return outperforms the avg8-step approach. Notably, the avg8-step method converges more rapidly, likely due to the stabilizing effect of averaging multiple updates.

Lastly, we compare GDRB with Hindsight Experience Replay (HER) Andrychowicz et al. (2017), a method for sparse-reward tasks that increases feedback to the agent by treating certain states in unsuccessful episodes as imaginary goals. By assigning rewards to these artificially generated goals, HER can leverage unsuccessful episodes more effectively. Figure 8 in Appendix A.3 compares the impact of GDRB and HER on DDPG in navigation environments. In *Wall-maze*, HER enables the agent to learn from previously unsuccessful trajectories, allowing it to achieve success rates above zero. In the other two environments, both GDRB and HER exhibit similar performance, although HER converges more quickly due to its reward-reshaping mechanism, which provides stronger guidance in the initial stages of training.

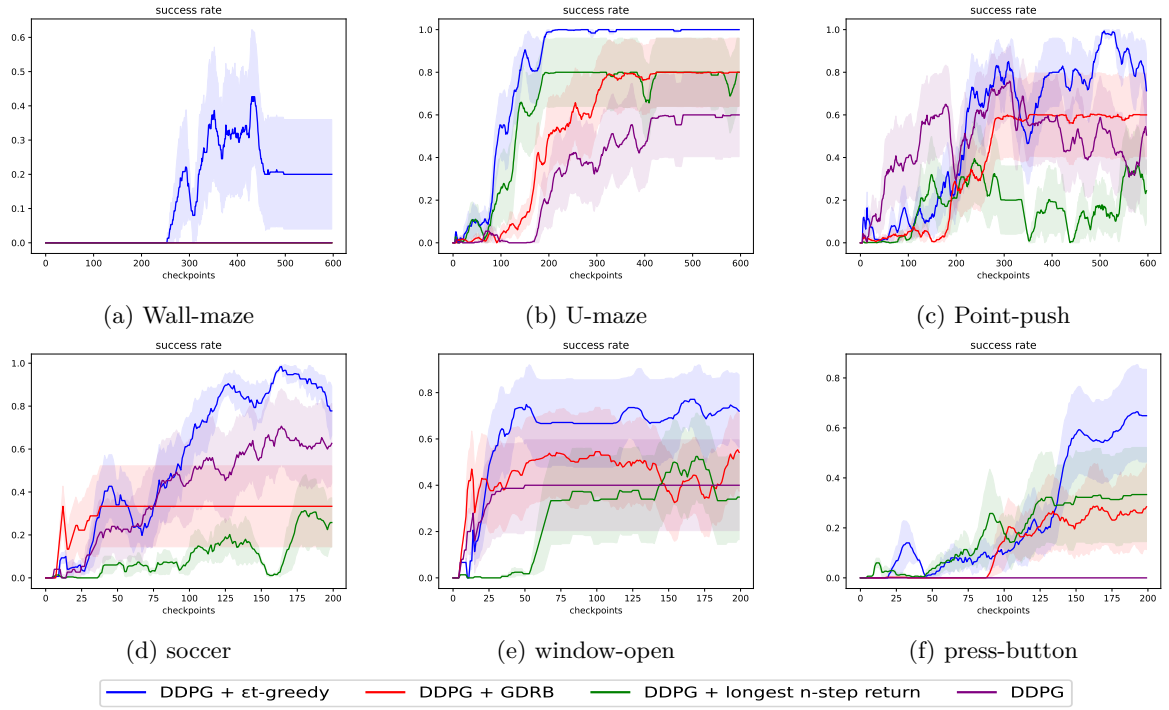

(a) Wall-maze (b) U-maze (c) Point-push

(d) soccer (e) window-open (f) press-button

Figure 7: Analyzing the individual impact of three components on DDPG: ϵt-greedy, GDRB, and longest n-step return.

5 Related Work

Intrinsic Motivation. Intrinsic motivation methods (Burda et al., 2018; Pathak et al., 2017; Ostrovski et al., 2017; Tang et al., 2017) provide a reward bonus for unexplored areas of the state space, enabling the agent to receive more feedback in sparse-reward scenarios. However, since a transition can receive varying rewards at different time steps, these methods make the reward function non-stationary, violating the Markov assumption of MDPs. They are also sensitive to hyperparameters, requiring extensive tuning for each environment (Schäfer et al., 2021). Decoupled RL algorithms (Schäfer et al., 2021; Badia et al., 2019) address this issue by training separate policies for exploration and exploitation, where the exploitation policy optimizes sparse rewards while leveraging data collected by the exploration policy. Although this resolves the non-stationarity issue, it doubles the computational cost. ϵt-greedy is similar to Tang et al. (2017) in identifying less-explored states using the SimHash function. However, unlike intrinsic motivation methods, ϵt-greedy does not modify the reward function. Instead, it directs the agent toward less-explored states, preserving the stationarity of the reward function while avoiding the need for additional computation.

Other Exploration Techniques. There are also other strategies to improve exploration without using reward bonuses. Colas et al. (2018) use a policy search process to generate diverse data to improve training of DDPG. Liu et al. (2018) introduce a competition-based exploration method where two agents (A and B) compete with each other. Agent A is penalized for visiting states visited by B, while B is rewarded for visiting states discovered by A. Plappert et al. (2018) directly inject noise into the policy's parameter space instead of the action space. Eysenbach et al. (2019) build a graph using states in the replay buffer, allowing the agent to navigate distant regions of the environment by applying Dijkstra's algorithm. ϵt-greedy shares similarities with Eysenbach et al. (2019) in constructing a tree structure within the state space. However, while Eysenbach et al. (2019) builds a single global graph to connect the start state to the goal state, ϵt-greedy generates local trees dynamically, focusing on accessing less-explored areas. Ecoffet et al. (2021) introduce *Go-Explore* which separates exploration and policy optimization into two distinct phases. During the exploration phase, the algorithm systematically explores the environment by maintaining an archive of

visited states along with their corresponding trajectories. In the robustification phase, these trajectories are leveraged to train a robust policy using standard reinforcement learning methods, such as PPO. However, a key limitation of Go-Explore is its reliance on resetting trajectories to return to previously visited states, a feature that is often unavailable in many real-world scenarios. Lobel et al. (2022) present Deep Optimistic Initialization for Exploration (DOIE), which improves exploration in continuous control tasks by maintaining optimism in state-action value estimates. Lobel et al. (2023) demonstrate that DOIE can estimate visit counts by averaging samples from the Rademacher distribution instead of using density models. Dey et al. (2024) present COIN, a continual optimistic initialization strategy that extends DOIE to stochastic and non-stationary environments. Chakraborty et al. (2023) leverage heavy-tailed action distributions to enhance exploration in continuous control tasks. Wang et al. (2022) propose a framework in which learned high-level policies select among a set of pre-designed low-level base controllers, allowing the agent to decompose complex long-horizon tasks into simpler control primitives. Dawood et al. (2023) use model predictive control (MPC), where a learned high-level policy proposes goals or waypoints, and MPC is used to generate low-level actions that guide the agent toward those goals.

Experience Replay Buffer. Rather than uniformly sampling from the buffer, Prioritized Experience Replay (PER) (Schaul et al., 2015) prioritizes transitions in the buffer based on reward, recency, or TD error at the expense of $O(\log N)$ per sample, where N is the buffer size. CER (Zhang & Sutton, 2017) includes the last transition from the buffer to each sampled batch with $O(1)$ complexity. Zhang et al. (2022) learn a conservative value regularizer only from the observed transitions in the replay buffer to improve the sample efficiency of DQN. Pan et al. (2022) theoretically show why PER has a better convergence rate than uniform sampling policy when minimizing mean squared error. Furthermore, Pan et al. (2022) identify two limitations of PER: outdated priorities and insufficient coverage of the state space. Kompella et al. (2023) propose Stratified Sampling from Event Tables (SSET), a method that partitions the experience replay buffer into distinct Event Tables. Each Event Table captures significant subsequences of optimal behavior, allowing for more targeted sampling during training. GDRB aligns conceptually with SSET if achieving a goal is defined as the sole event. However, SSET employs FIFO for inserting new data into its buffers, whereas GDRB uses reservoir sampling for its success-event buffer. Moreover, in SSET, the sampling ratios between buffers are fixed, while GDRB dynamically adjusts these ratios over time to favor the smaller buffer.

Reward Propagation. Reward shaping (Laud, 2004; Hu et al., 2020) creates artificial intermediate rewards to facilitate reward propagation. However, designing appropriate intermediate rewards is hard and often problem-specific. Trott et al. (2019) address this issue by introducing *self-balancing reward shaping* in the context of on-policy learning. Their approach defines the local optimum as the closest visited state to the goal and calculates the reward for each state based on its distance from the local optimum and the goal. By dynamically adjusting the local optimum, the agent is guided toward the optimal behavior. To extract more information from an unsuccessful episode, Andrychowicz et al. (2017) introduce *imaginary goals*. An imaginary goal for state s is a state that is encountered later in the episode. Learning to achieve these imaginary goals helps the agent understand the structure of the environment. Memarian et al. propose *Self-Supervised Online Reward Shaping (SORS)*, a method that alternates between ranking trajectories using sparse rewards and training a classifier to infer a dense reward function from these rankings. The inferred dense rewards are then utilized to update the agent's policy. Devidze et al. (2024) present a reward informativeness criterion that adaptively constructs interpretable reward functions based on the agent's current policy. Wilcox et al. (2022) propose a Monte Carlo Augmented Actor-Critic (MCA2C) framework that integrates Monte Carlo returns from suboptimal demonstration trajectories into the critic update to improve value estimation in sparse-reward settings. By combining temporal-difference targets with demonstration-based Monte Carlo returns, the method provides more informative learning signals during early training, enabling the agent to better propagate sparse rewards.

6 Conclusions and Future Work

We have introduced the ETGL-DDPG algorithm with three orthogonal components that improve the performance of DDPG for sparse-reward goal-conditioned environments. ϵt-greedy is a temporally-extended version of ϵ-greedy using options generated by search. We prove that ϵt-greedy achieves a polynomial sample complexity under specific MDP structural assumptions. GDRB employs an extra buffer to separate success-

ful episodes. The longest n-step return bootstraps from the Q-value of the final state in unsuccessful episodes and becomes a Monte Carlo update in successful episodes. ETGL-DDPG uses these components with DDPG and outperforms state-of-the-art methods, at the expense of about 1.5x wall-clock time w.r.t DDPG. The current limitation of our work is that we approximate visit counts through static hashing. For image-based problems such as real-world navigation, the future direction is to leverage dynamic hashing techniques such as *normalizing flows* (Papamakarios et al., 2021) as these tasks demand more intricate representation learning. Additionally, ϵt-greedy and GDRB are designed for deterministic domains and would require adaptation for stochastic environments. Extending these components to stochastic domains represents another promising direction for future research.

References

Marcin Andrychowicz, Filip Wolski, Alex Ray, Jonas Schneider, Rachel Fong, Peter Welinder, Bob McGrew, Josh Tobin, OpenAI Pieter Abbeel, and Wojciech Zaremba. Hindsight experience replay. *Advances in Neural Information Processing Systems*, 30, 2017.

Kavosh Asadi, Neev Parikh, Ronald E Parr, George D Konidaris, and Michael L Littman. Deep radial-basis value functions for continuous control. In *Proceedings of the AAAI Conference on Artificial Intelligence*, volume 35, pp. 6696–6704, 2021.

Adrià Puigdomènech Badia, Pablo Sprechmann, Alex Vitvitskyi, Daniel Guo, Bilal Piot, Steven Kapturowski, Olivier Tieleman, Martin Arjovsky, Alexander Pritzel, Andrew Bolt, et al. Never give up: Learning directed exploration strategies. In *International Conference on Learning Representations*, 2019.

Andrea Baronchelli and Filippo Radicchi. Lévy flights in human behavior and cognition. *Chaos, Solitons & Fractals*, 56:101–105, 2013.

Gabriel Barth-Maron, Matthew W. Hoffman, David Budden, Will Dabney, Dan Horgan, Dhruva TB, Alistair Muldal, Nicolas Heess, and Timothy P. Lillicrap. Distributed distributional deterministic policy gradients. In *6th International Conference on Learning Representations, ICLR 2018, Vancouver, BC, Canada, April 30 - May 3, 2018, Conference Track Proceedings*. OpenReview.net, 2018. URL `https://openreview.net/forum?id=SyZipzbCb`.

Burton H Bloom. Space/time trade-offs in hash coding with allowable errors. *Communications of the ACM*, 13(7):422–426, 1970.

Yuri Burda, Harrison Edwards, Amos Storkey, and Oleg Klimov. Exploration by random network distillation. In *International Conference on Learning Representations*, 2018.

Souradip Chakraborty, Amrit Singh Bedi, Kasun Weerakoon, Prithvi Poddar, Alec Koppel, Pratap Tokekar, and Dinesh Manocha. Dealing with sparse rewards in continuous control robotics via heavy-tailed policy optimization. In *2023 IEEE International Conference on Robotics and Automation (ICRA)*, pp. 989–995. IEEE, 2023.

Moses S Charikar. Similarity estimation techniques from rounding algorithms. In *Proceedings of the thiry-fourth annual ACM symposium on Theory of computing*, pp. 380–388, 2002.

Cédric Colas, Olivier Sigaud, and Pierre-Yves Oudeyer. GEP-PG: Decoupling exploration and exploitation in deep reinforcement learning algorithms. In *International Conference on Machine Learning*, pp. 1039–1048. PMLR, 2018.

Will Dabney, Georg Ostrovski, and Andre Barreto. Temporally-extended ε-greedy exploration. In *International Conference on Learning Representations*, 2020.

Murad Dawood, Nils Dengler, Jorge de Heuvel, and Maren Bennewitz. Handling sparse rewards in reinforcement learning using model predictive control. In *2023 IEEE International Conference on Robotics and Automation (ICRA)*, pp. 879–885. IEEE, 2023.

Rati Devidze, Parameswaran Kamalaruban, and Adish Singla. Informativeness of reward functions in reinforcement learning. In *23rd International Conference on Autonomous Agents and Multiagent Systems*, pp. 444–452. ACM, 2024.

Sheelabhadra Dey, James Ault, and Guni Sharon. Continual optimistic initialization for value-based reinforcement learning. In *Proceedings of the 23rd International Conference on Autonomous Agents and Multiagent Systems*, pp. 453–462, 2024.

Prafulla Dhariwal, Christopher Hesse, Oleg Klimov, Alex Nichol, Matthias Plappert, Alec Radford, John Schulman, Szymon Sidor, Yuhuai Wu, and Peter Zhokhov. OpenAI baselines. `https://github.com/openai/baselines`, 2017.

Yan Duan, Xi Chen, Rein Houthooft, John Schulman, and Pieter Abbeel. Benchmarking deep reinforcement learning for continuous control. In *International conference on machine learning*, pp. 1329–1338. PMLR, 2016.

Adrien Ecoffet, Joost Huizinga, Joel Lehman, Kenneth O Stanley, and Jeff Clune. First return, then explore. *Nature*, 590(7847):580–586, 2021.

Eyal Even-Dar and Yishay Mansour. Learning rates for q-learning. *J. Mach. Learn. Res.*, 5:1–25, December 2004. ISSN 1532-4435.

Ben Eysenbach, Russ R Salakhutdinov, and Sergey Levine. Search on the replay buffer: Bridging planning and reinforcement learning. *Advances in Neural Information Processing Systems*, 32, 2019.

Scott Fujimoto, Herke Hoof, and David Meger. Addressing function approximation error in actor-critic methods. In *International Conference on Machine Learning*, pp. 1587–1596. PMLR, 2018.

Tuomas Haarnoja, Aurick Zhou, Pieter Abbeel, and Sergey Levine. Soft actor-critic: Off-policy maximum entropy deep reinforcement learning with a stochastic actor. In *International Conference on Machine Learning*, pp. 1861–1870. PMLR, 2018.

Matteo Hessel, Joseph Modayil, Hado Van Hasselt, Tom Schaul, Georg Ostrovski, Will Dabney, Dan Horgan, Bilal Piot, Mohammad Azar, and David Silver. Rainbow: Combining improvements in deep reinforcement learning. In *Proceedings of the AAAI conference on artificial intelligence*, volume 32, 2018.

Yujing Hu, Weixun Wang, Hangtian Jia, Yixiang Wang, Yingfeng Chen, Jianye Hao, Feng Wu, and Changjie Fan. Learning to utilize shaping rewards: A new approach of reward shaping. *Advances in Neural Information Processing Systems*, 33:15931–15941, 2020.

Sham M. Kakade. On the sample complexity of reinforcement learning. 2003. URL `https://api.semanticscholar.org/CorpusID:260534783`.

Yuji Kanagawa. mujoco-maze. `https://github.com/kngwyu/mujoco-maze`, 2021.

B Ravi Kiran, Ibrahim Sobh, Victor Talpaert, Patrick Mannion, Ahmad A Al Sallab, Senthil Yogamani, and Patrick Pérez. Deep reinforcement learning for autonomous driving: A survey. *IEEE Transactions on Intelligent Transportation Systems*, 23(6):4909–4926, 2021.

Varun Raj Kompella, Thomas Walsh, Samuel Barrett, Peter R. Wurman, and Peter Stone. Event tables for efficient experience replay. *Transactions on Machine Learning Research*, 2023. ISSN 2835-8856. URL `https://openreview.net/forum?id=XejzjAjKjv`.

Adam Daniel Laud. *Theory and application of reward shaping in reinforcement learning*. University of Illinois at Urbana-Champaign, 2004.

Steven LaValle. Rapidly-exploring random trees: A new tool for path planning. *Research Report 9811*, 1998.

Joel Lehman, Jay Chen, Jeff Clune, and Kenneth O Stanley. ES is more than just a traditional finite-difference approximator. In *Proceedings of the genetic and evolutionary computation conference*, pp. 450–457, 2018.

Timothy P Lillicrap, Jonathan J Hunt, Alexander Pritzel, Nicolas Heess, Tom Erez, Yuval Tassa, David Silver, and Daan Wierstra. Continuous control with deep reinforcement learning. *arXiv preprint arXiv:1509.02971*, 2015.

Bo Liu, Yihao Feng, Qiang Liu, and Peter Stone. Metric residual network for sample efficient goal-conditioned reinforcement learning. In *Proceedings of the AAAI Conference on Artificial Intelligence*, volume 37, pp. 8799–8806, 2023.

Hao Liu, Alexander Trott, Richard Socher, and Caiming Xiong. Competitive experience replay. In *International Conference on Learning Representations*, 2018.

Yao Liu and Emma Brunskill. When simple exploration is sample efficient: Identifying sufficient conditions for random exploration to yield PAC RL algorithms. *CoRR*, abs/1805.09045, 2018.

Sam Lobel, Omer Gottesman, Cameron Allen, Akhil Bagaria, and George Konidaris. Optimistic initialization for exploration in continuous control. In *Proceedings of the AAAI Conference on Artificial Intelligence*, volume 36, pp. 7612–7619, 2022.

Sam Lobel, Akhil Bagaria, and George Konidaris. Flipping coins to estimate pseudocounts for exploration in reinforcement learning. In *International Conference on Machine Learning*, pp. 22594–22613. PMLR, 2023.

Kevin Sebastian Luck, Mel Vecerik, Simon Stepputtis, Heni Ben Amor, and Jonathan Scholz. Improved exploration through latent trajectory optimization in deep deterministic policy gradient. In *2019 IEEE/RSJ International Conference on Intelligent Robots and Systems (IROS)*, pp. 3704–3711. IEEE, 2019.

Guillaume Matheron, Nicolas Perrin, and Olivier Sigaud. The problem with DDPG: understanding failures in deterministic environments with sparse rewards. *arXiv preprint arXiv:1911.11679*, 2019.

Farzan Memarian, Wonjoon Goo, Rudolf Lioutikov, Scott Niekum, and Ufuk Topcu. Self-supervised online reward shaping in sparse-reward environments. in 2021 ieee. In *RSJ International Conference on Intelligent Robots and Systems (IROS)*, pp. 2369–2375.

Lingheng Meng, Rob Gorbet, and Dana Kulić. The effect of multi-step methods on overestimation in deep reinforcement learning. In *2020 25th International Conference on Pattern Recognition (ICPR)*, pp. 347–353. IEEE, 2021.

Volodymyr Mnih, Koray Kavukcuoglu, David Silver, Alex Graves, Ioannis Antonoglou, Daan Wierstra, and Martin Riedmiller. Playing atari with deep reinforcement learning. *arXiv preprint arXiv:1312.5602*, 2013.

Volodymyr Mnih, Adria Puigdomenech Badia, Mehdi Mirza, Alex Graves, Timothy Lillicrap, Tim Harley, David Silver, and Koray Kavukcuoglu. Asynchronous methods for deep reinforcement learning. In *International Conference on Machine Learning*, pp. 1928–1937. PMLR, 2016.

Georg Ostrovski, Marc G Bellemare, Aäron Oord, and Rémi Munos. Count-based exploration with neural density models. In *International Conference on Machine Learning*, pp. 2721–2730. PMLR, 2017.

Ling Pan, Qingpeng Cai, and Longbo Huang. Softmax deep double deterministic policy gradients. *Advances in neural information processing systems*, 33:11767–11777, 2020.

Yangchen Pan, Jincheng Mei, Amir-massoud Farahmand, Martha White, Hengshuai Yao, Mohsen Rohani, and Jun Luo. Understanding and mitigating the limitations of prioritized experience replay. In *Uncertainty in Artificial Intelligence*, pp. 1561–1571. PMLR, 2022.

George Papamakarios, Eric Nalisnick, Danilo Jimenez Rezende, Shakir Mohamed, and Balaji Lakshminarayanan. Normalizing flows for probabilistic modeling and inference. *The Journal of Machine Learning Research*, 22(1):2617–2680, 2021.

Deepak Pathak, Pulkit Agrawal, Alexei A Efros, and Trevor Darrell. Curiosity-driven exploration by self-supervised prediction. In *International Conference on Machine Learning*, pp. 2778–2787. PMLR, 2017.

Matthias Plappert, Rein Houthooft, Prafulla Dhariwal, Szymon Sidor, Richard Y Chen, Xi Chen, Tamim Asfour, Pieter Abbeel, and Marcin Andrychowicz. Parameter space noise for exploration. In *International Conference on Learning Representations*, 2018.

Lukas Schäfer, Filippos Christianos, Josiah P Hanna, and Stefano V Albrecht. Decoupled reinforcement learning to stabilise intrinsically-motivated exploration. *arXiv preprint arXiv:2107.08966*, 2021.

Tom Schaul, John Quan, Ioannis Antonoglou, and David Silver. Prioritized experience replay. *arXiv preprint arXiv:1511.05952*, 2015.

David Silver, Guy Lever, Nicolas Heess, Thomas Degris, Daan Wierstra, and Martin Riedmiller. Deterministic policy gradient algorithms. In *International Conference on Machine Learning*, pp. 387–395. PMLR, 2014.

Richard S Sutton and Andrew G Barto. *Reinforcement learning: An introduction*. MIT press, 2018.

Richard S Sutton, Doina Precup, and Satinder Singh. Between MDPs and semi-MDPs: A framework for temporal abstraction in reinforcement learning. *Artificial intelligence*, 112(1-2):181–211, 1999.

Haoran Tang, Rein Houthooft, Davis Foote, Adam Stooke, OpenAI Xi Chen, Yan Duan, John Schulman, Filip DeTurck, and Pieter Abbeel. # exploration: A study of count-based exploration for deep reinforcement learning. *Advances in neural information processing systems*, 30, 2017.

Sebastian Thrun and Anton Schwartz. Issues in using function approximation for reinforcement learning. In *Proceedings of the Fourth Connectionist Models Summer School*, volume 255, pp. 263. Hillsdale, NJ, 1993.

Daniil Tiapkin, Nikita Morozov, Alexey Naumov, and Dmitry P Vetrov. Generative flow networks as entropy-regularized rl. In *International Conference on Artificial Intelligence and Statistics*, pp. 4213–4221. PMLR, 2024.

Emanuel Todorov, Tom Erez, and Yuval Tassa. Mujoco: A physics engine for model-based control. In *2012 IEEE/RSJ International Conference on Intelligent Robots and Systems*, pp. 5026–5033. IEEE, 2012.

Alexander Trott, Stephan Zheng, Caiming Xiong, and Richard Socher. Keeping your distance: Solving sparse reward tasks using self-balancing shaped rewards. *Advances in Neural Information Processing Systems*, 32, 2019.

George E Uhlenbeck and Leonard S Ornstein. On the theory of the Brownian motion. *Physical review*, 36 (5):823, 1930.

Jeffrey S Vitter. Random sampling with a reservoir. *ACM Transactions on Mathematical Software (TOMS)*, 11(1):37–57, 1985.

Guangming Wang, Minjian Xin, Wenhua Wu, Zhe Liu, and Hesheng Wang. Learning of long-horizon sparse-reward robotic manipulator tasks with base controllers. *IEEE Transactions on Neural Networks and Learning Systems*, 35(3):4072–4081, 2022.

Tongzhou Wang, Antonio Torralba, Phillip Isola, and Amy Zhang. Optimal goal-reaching reinforcement learning via quasimetric learning. In *International Conference on Machine Learning*, pp. 36411–36430. PMLR, 2023.

Albert Wilcox, Ashwin Balakrishna, Jules Dedieu, Wyame Benslimane, Daniel Brown, and Ken Goldberg. Monte carlo augmented actor-critic for sparse reward deep reinforcement learning from suboptimal demonstrations. *Advances in neural information processing systems*, 35:2254–2267, 2022.

Tianhe Yu, Deirdre Quillen, Zhanpeng He, Ryan Julian, Karol Hausman, Chelsea Finn, and Sergey Levine. Meta-world: A benchmark and evaluation for multi-task and meta reinforcement learning. In *Conference on Robot Learning*, pp. 1094–1100. PMLR, 2020.

Hongming Zhang, Chenjun Xiao, Han Wang, Jun Jin, Martin Müller, et al. Replay memory as an empirical mdp: Combining conservative estimation with experience replay. In *The Eleventh International Conference on Learning Representations*, 2022.

Linjing Zhang, Zongzhang Zhang, Zhiyuan Pan, Yingfeng Chen, Jiangcheng Zhu, Zhaorong Wang, Meng Wang, and Changjie Fan. A framework of dual replay buffer: balancing forgetting and generalization in reinforcement learning. In *Proceedings of the 2nd Workshop on Scaling Up Reinforcement Learning (SURL), International Joint Conference on Artificial Intelligence (IJCAI)*, 2019.

Shangtong Zhang and Richard S Sutton. A deeper look at experience replay. *arXiv preprint arXiv:1712.01275*, 2017.

A Appendix

A.1 ϵt-greedy Sample Efficiency : Proofs

In this section, we first provide an overview of the proof, presenting the key ideas at a high level. Then, we present the detailed formal proof of Theorem 1 and Theorem 2.

Proof Overview. We aim to show that the ϵt-greedy algorithm falls into the PAC-MDP category. According to Liu & Brunskill (2018), an algorithm $\mathcal{A}$ is PAC-MDP if the covering time induced by $\mathcal{A}$ is polynomially bounded. In Liu & Brunskill (2018), the authors further demonstrate that bounding the covering time requires bounding both the Laplacian eigenvalues and the stationary distribution over the states induced by the random walk policy. This is presented as Proposition A.1. According to Theorem 2, two conditions are satisfied: $N \leq \Theta(|\mathcal{S}||\mathcal{A}|)$ and a lower bound on the probability of the sampled option, $\mathcal{P}_{\mathcal{X}} \geq \frac{1}{\Theta(|\mathcal{S}||\mathcal{A}|)}$. These two conditions are necessary and are met by our problem setting and the exploration algorithm (Algorithm 1). To prove that $\mathcal{P}_{\mathcal{X}} \geq \frac{1}{\Theta(|\mathcal{S}||\mathcal{A}|)}$, we construct a worst-case tree structure $\mathcal{X}$, where we aim to identify the option induced by the tree $\mathcal{X}$ with the lowest probability, referred to informally as the "hardest option". We then show that this lower bound satisfies the condition specified in Theorem 1.

We now proceed with the proof of Theorem 1, as demonstrated below.

Theorem 1 (**Worst-Case Sampling**). *Given a tree $\mathcal{X}$ with N nodes (s_1 to s_N), for any $\omega \in \Omega_{\mathcal{X}}$, the sampling probability satisfies:*

$$\mathcal{P}_{\mathcal{X}}[\omega] \geq \frac{1}{N!(\max_{i\in[N]} |\phi(s_i)|)^{N-1}} \geq \frac{1}{\Theta(|\mathcal{S}||\mathcal{A}|)} \tag{7}$$

where $N \leq \frac{\log(|\mathcal{S}||\mathcal{A}|)}{\log\log(|\mathcal{S}||\mathcal{A}|)}$ Here, $\mathcal{S}$ and $\mathcal{A}$ represent the state space and action space, respectively.

Proof. As outlined in the proof overview, we need to construct an option with the lowest sampling probability. Given a tree $\mathcal{X}$, we define $\mathcal{X}_i$ (for $1 \leq i \leq N$) as the tree constructed up to the i-th time step. At each step $\mathcal{X}_i$, we track the tuple of added states, denoted by $\mathcal{S}_i^{\mathcal{X}}$, the uniformly sampled state s_x from $\mathcal{S}_i^{\mathcal{X}}$, and the state with the fewest visits, s_{min}. The notation s_x and s_{min} follows Algorithm 1. Without loss of generality, we assume that each next state $s_{x'}$ in line 9 of Algorithm 1 satisfies $n(\phi(s_{x'})) \neq 0$. Specifically, we consider a worst-case tree $\mathcal{X}$ fully populated with states from s_1 to s_N. Therefore, at time step N, $\mathcal{S}_N^{\mathcal{X}} = (s_1, s_2, \ldots, s_N)$, and we have the following relation:

$$n(\phi(s_1)) \geq n(\phi(s_2)) \geq n(\phi(s_3)) \cdots \geq n(\phi(s_N)). \tag{8}$$

Equation 8 provides a decreasing sequence of visitations for newly added nodes in tree $\mathcal{X}$, emphasizing line 15 of Algorithm 1, which causes the state s_{min} to change over N iterations. We assume a specific structure for each $\phi(s_i)$, where for all $i \in [N]$, at each bucket $\phi(s_i)$, there exists only one state denoted by s_{i+1}, such that $n(\phi(s_{i+1})) \leq n(\phi(s_i))$. Additionally, we assume that at each time step in $\mathcal{X}_t$, the newly added node connects only to the most recently added node in the tree. The two key stochastic events are summarized as follows:

- $\mathcal{E}_1$: The event in which nodes are sampled in Line 24 from buckets satisfying the increasing sequence above.
- $\mathcal{E}_2$: The event in which nodes are selected in Line 8.

We now define the probability of interest, which we aim to bound:

$$\mathcal{P}[\text{option returned from } s_{\text{root}} \text{ to } s_N | \mathcal{E}_1 \text{ and } \mathcal{E}_2]. \tag{9}$$

We expand this probability as follows:

$$\begin{aligned}
\mathcal{P}[\text{option returned from } s_{\text{root}} \text{ to } s_N \mid \mathcal{E}_1 \text{ and } \mathcal{E}_2] &= \prod_{i=2}^{N} \mathcal{P}[(\text{State } s_i \text{ added to tree } \mathcal{X}) \wedge (s_i = s_{min}) \wedge (s_x = s_{i-1} \text{ in Line 8})] \\
&= \prod_{i=2}^{N} \frac{1}{(i-1)|\phi(s_{i-1})|} \\
&= \frac{1}{(N-1)!} \times \frac{1}{|\phi(s_1)||\phi(s_2)| \dots |\phi(s_N)|} \\
&> \frac{1}{N!} \times \frac{1}{(\max_{i\in[N]} |\phi(s_i)|)^{N-1}} \\
&> \frac{1}{|\mathcal{S}||\mathcal{A}|}.
\end{aligned}$$

To prove the final inequality, note that $N \leq \frac{\log(|\mathcal{S}||\mathcal{A}|)}{\log\log(|\mathcal{S}||\mathcal{A}|)}$. Since the size of the sets $\mathcal{S}$ and $\mathcal{A}$ is large and N is sub-logarithmic in $|\mathcal{S}||\mathcal{A}|$, i.e., $N \ll \log(|\mathcal{S}||\mathcal{A}|)$, we can say $N \leq \frac{\log(|\mathcal{S}||\mathcal{A}|)}{\log(N)}$. Let us denote $\log(\max_{i\in[N]} |\phi(s_i)|)$ as a constant c_0.

Now by the series of following inequalities we prove that $\frac{1}{N!} \times \frac{1}{(\max_{i\in[N]} |\phi(s_i)|)^{N-1}} > \frac{1}{|\mathcal{S}||\mathcal{A}|}$.

$$N \leq \frac{\log(|\mathcal{S}||\mathcal{A}|)}{\log(N)} \Rightarrow N\log(N) \leq \log(|\mathcal{S}||\mathcal{A}|) \tag{10}$$

$$\Rightarrow N\log(N) + (N-1)c_0 - N \leq \log(|\mathcal{S}||\mathcal{A}|) \qquad (\text{since } |\mathcal{S}||\mathcal{A}| \gg N, c_0) \tag{11}$$

$$\Rightarrow \log(N!) + (N-1)c_0 \leq \log(|\mathcal{S}||\mathcal{A}|) \qquad (\text{Based on the Moivre–Stirling approximation}) \tag{12}$$

$$\Rightarrow \log(N!) + (N-1)c_0 \leq \log(|\mathcal{S}||\mathcal{A}|) \tag{13}$$

$$\Rightarrow \log(N!) + \log\left((\max_{i\in[N]} |\phi(s_i)|)^{N-1}\right) \leq \log(|\mathcal{S}||\mathcal{A}|) \tag{14}$$

$$\Rightarrow \log\left(N! \cdot (\max_{i\in[N]} |\phi(s_i)|)^{N-1}\right) \leq \log(|\mathcal{S}||\mathcal{A}|) \tag{15}$$

$$\Rightarrow \frac{1}{N! \cdot (\max_{i\in[N]} |\phi(s_i)|)^{N-1}} \geq \frac{1}{|\mathcal{S}||\mathcal{A}|} \tag{16}$$

□

Now we provide the main proof which demonstrates polynomial sample complexity under certain criteria.

Theorem 2 (**ϵt-greedy Sample Efficiency**). *Given a state space $\mathcal{S}$, action space $\mathcal{A}$, and a set of options $\Omega_{\mathcal{X}}$ generated by ϵt-greedy for each tree $\mathcal{X}$, if $\mathcal{P}_{\mathcal{X}}[\omega] \geq \frac{1}{\Theta(|\mathcal{S}||\mathcal{A}|)}$, ϵt-greedy achieves polynomial sample complexity or i.e. is PAC-MDP.*

Proof. First note that if $\mathcal{P}_{\mathcal{X}}[\omega] \geq \frac{1}{\Theta(|\mathcal{S}||\mathcal{A}|)}$ then based on Theorem 1 we need to have $N \leq \frac{\log(|\mathcal{S}||\mathcal{A}|)}{\log\log(|\mathcal{S}||\mathcal{A}|)}$, and this implies that $N \leq \Theta(|\mathcal{S}||\mathcal{A}|)$. Based on the paper by (Liu & Brunskill, 2018), and the analysis of the covering length when following a random policy, we have the following preposition:

Preposition A.1 (**Liu & Brunskill (2018)**). *: For any irreducable MDP M, we define $P_{\pi_{RW}}$ as a transition matrix induced by random walk policy π_{RW} over M and $L(P_{\pi_{RW}})$ is denoted as the Laplacian of this transition matrix. Suppose λ is the smallest non-zero eigenvalue of L and $\Psi(s)$ is the stationary distribution over states which is induced by random walk policy, then Q-learning with random walk exploration is a PAC RL algorithm if: $\frac{1}{\lambda}, \frac{1}{\min_s \Psi(s)}$ are Poly($|\mathcal{S}||\mathcal{A}|$).*

Note that Preposition A.1 is not limited to an MDP with primitive actions. Therefore, we can broaden its scope by incorporating options into this proposition and demonstrate that both $\frac{1}{\lambda}$ and $\frac{1}{\min_s \Psi(s)}$ can be polynomially bounded in terms of MDP parameters—in this case, states and actions in our approach.

Let's begin by examining the upper-bound for $\frac{1}{\min_s \Psi(s)}$. Suppose we are at exploration tree $\mathcal{X}$. Without a loss of generality, we consider that capacity of tree $\mathcal{X}$ is full, and we have N states. In this tree, let's designate s_{root} as the state assigned as the root of the tree during the exploration phase. Now, consider another random state (excluding s_{root}) within this tree structure, denoted as s_{rand}. We acknowledge that, when considering the entire state space, there can be multiple options constructed from s_{root} to s_{rand}. Each tree $\mathcal{X}$ provides one of these options. $\Psi(s)$ is defined over all states, and ω is the option with a limited size because of the constrained tree budget.

we can calculate the upper-bound for $\frac{1}{\min_s \Psi(s)}$ as follows:

$$\begin{aligned} \Psi(s_{rand}) = \sum_{\omega \in \Omega_{\mathcal{X}}} \mathcal{P}_{\mathcal{X}}[\omega]\Psi(s_{root}) \Rightarrow \Psi(s_{rand}) \geq \mathcal{P}[\omega]\Psi(s_{root}), \\ \frac{1}{\Psi(s_{rand})} \leq \frac{1}{\mathcal{P}[\omega]} \frac{1}{\Psi(s_{root})} \Rightarrow \frac{1}{\Psi(s_{rand})} \leq \frac{\Theta(|\mathcal{S}||\mathcal{A}|)}{\Psi(s_{root})} \end{aligned} \tag{17}$$

Since s_{rand} can represent any of the states encountered in the tree, we can regard it as the state assigned the least probability in the stationary distribution. Therefore, we have:

$$\frac{1}{\Psi(s_{rand})} \leq \frac{\Theta(|\mathcal{S}||\mathcal{A}|)}{\Psi(s_{root})} \Rightarrow \frac{1}{\min_s \Psi(s)} \leq \frac{\Theta(|\mathcal{S}||\mathcal{A}|)}{\Psi(s_{root})} \tag{18}$$

So, $\frac{1}{\min_s \Psi(s)}$ is polynomially bounded. Now, we need to demonstrate that $\frac{1}{\lambda}$ is also polynomially bounded. To bound λ, we first need to recall the definition of the Cheeger constant, h. Drawing from graph theory, if we denote $V(G)$ and $E(G)$ as the set of vertices and edges of an undirected graph G, respectively, and considering the subset of vertices denoted by V_s, we can define σV_s as follows:

$$\sigma V_s := \{(n_1, n_2) \in E(G) : n_1 \in V_s, n_2 \in V(G) \setminus V_s\} \tag{19}$$

So, σV_s can be regarded as a collection of all edges going from V_s to the vertex set outside of V_s. In the above definition, (n_1, n_2) is considered as a graph edge. Now, we can define a Cheeger constant:

$$h(G) := \min\{\frac{|\sigma V_s|}{|V_s|} : V_s \subseteq V(G), 0 < V_s \leq \frac{1}{2}|V(G)|\} \tag{20}$$

We are aware that $h \geq \lambda \geq \frac{h^2}{2}$, and by polynomially bounding h, we can ensure that λ is also bounded. In a related work (Liu & Brunskill, 2018), an alternative variation of the Cheeger constant is utilized, which is based on the flow F induced by the stationary distribution Ψ of a random walk on the graph. Suppose for nodes n_1, n_2 and subset of nodes N_1 in the graph, we have:

$$F(n_1, n_2) = \Psi(n_1)P(n_1, n_2), \tag{21}$$

$$F(\sigma N_1) = \sum_{n_1 \in N_1, n_2 \notin N_1} F(n_1, n_2), \tag{22}$$

$$F(N_1) = \sum_{n_1 \in N_1} \Psi(n_1) \tag{23}$$

Building upon the aforementioned definition, the Cheeger constant is defined as:

$$h := \inf_{N_1} \frac{F(\sigma N_1)}{\min\{F(N_1), F(\bar{N_1})\}} \tag{24}$$

Suppose $N_{rand} = \{s_{root}\}$; we will now demonstrate that $\frac{1}{h}$ can be polynomially bounded :

$$h = \inf_{N_1} \frac{F(\sigma N_1)}{\min\{F(N_1), F(\bar{N_1})\}} \geq \frac{F(\sigma N_{rand})}{\min\{F(N_{rand}), F(\overline{N_{rand}})\}} \geq \frac{\sum_{s \neq s_{root}} \Psi(s_{root}) P_{\pi_{RW}}(s_{root}, s)}{\Psi(s_{root})},$$
$$= \sum_{s \neq S_{root}} P_{\pi_{RW}}(s_{root}, s) \geq \mathcal{P}_{\mathcal{X}}[\omega] \Rightarrow \frac{1}{h} \leq \Theta(|\mathcal{S}||\mathcal{A}|)$$

We demonstrate that both terms stated in Preposition A.1 are polynomially bounded, and thus, the proof is complete. □

Algorithm 2 Generating exploratory option with tree search using a perfect model

```
function generate_option(state s, hash function φ, budget N)
    frontier_nodes ← {}
    Initialize root using s: root ← TreeNode(s)
    frontier_nodes ← frontier_nodes ∪ {root};
    s_min ← root
    i ← 0
    while i < N do
        s_x ∼ UniformRandom(frontier_nodes)
        s_x' = next_state_from_env(s_x)
        if φ(n(s_x'))=0 then
            Extract option o by actions root to s_x'
            return o
        end if
        if n(φ(s_x')) < n(φ(s_min)) then
            s_min=s_x'
        end if
        i ← i + 1
    end while
    Extract option o by actions root to s_min
    return o
end function

function next_state_from_env(s_x, frontier_nodes)
    a ∼ UniformRandom(A(s_x))
    s_x' ← T(s_x, a)
    s_x.add_child (s_x')
    frontier_nodes ← frontier_nodes ∪ {s_x'}
    return s_x'
end function
```

A.2 n-step Methods Comparison

In this section, we compare two update rules for Q-values in DDPG: the longest n-step return and the average return over 1 to 8 steps (avg8-step). The results are shown in Figure 9. Both methods performed similarly overall; however, in the Wall-maze environment, the longest n-step return outperformed the avg8-step approach. The avg8-step method converged more quickly in U-maze and Point-push due to the stabilizing effect of averaging multiple updates.

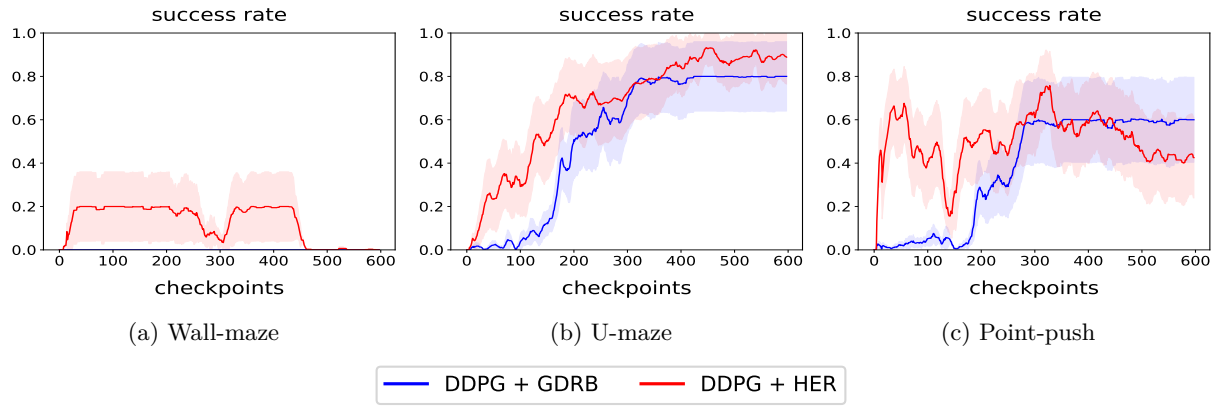

(a) Wall-maze (b) U-maze (c) Point-push

Figure 8: The comparison between two replay buffer strategies: GDRB and HER.

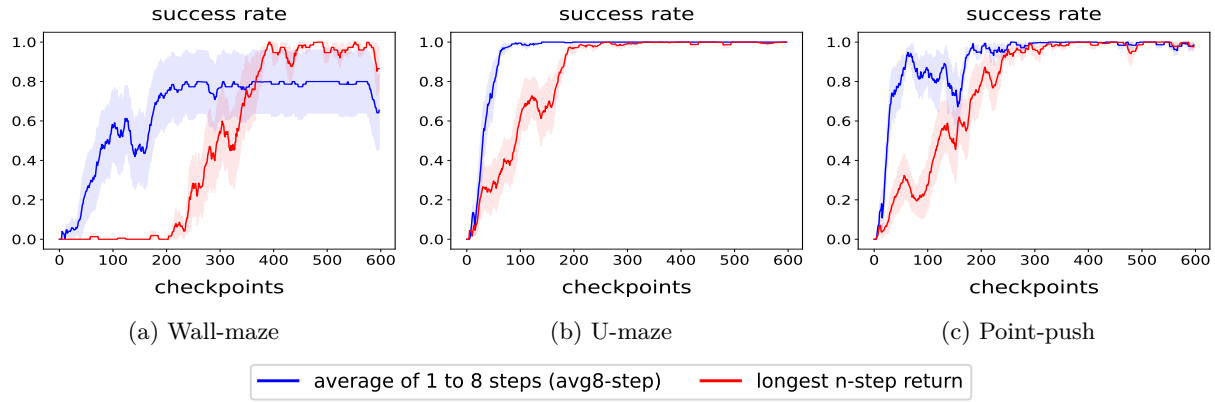

(a) Wall-maze (b) U-maze (c) Point-push

Figure 9: The comparison between two update rules for Q-values: the longest n-step return and the average return over 1 to 8 steps (avg8-step).

A.3 Comparison of GDRB and Hindsight Experience Replay (HER)

In this section, we compare two strategies for storing transitions in the replay buffer: GDRB and HER. Figure 8 shows the results in the navigation environments. In Wall-maze, HER achieves success rates above zero during the early stages of training; however, it fails to maintain any success in later stages. This observation is consistent with the results reported by Trott et al. (2019) in the same environment. In the other two environments, both methods exhibit comparable performance, but HER discovers paths to the goal more quickly, as it leverages reward shaping in unsuccessful episodes to provide additional information about the structure of the environment.

A.4 Exploration with a Perfect Model

Since the DDPG algorithm is model-free, we utilize the replay buffer to construct the tree for ϵt-greedy. However, ϵt-greedy can also take advantage of a perfect model when available. The pseudocode for option generation using a perfect model is provided in Algorithm 2. The key difference from Algorithm 1 is the use of the `next_state_from_env` function instead of `next_state_from_replay_buffer` to generate child nodes. In this case, an action is uniformly sampled from the action space, and the environment's transition function $\mathcal{T}$ is directly used to determine the next state (line 25). Figure 10 compares the performance of ETGL-DDPG in navigation environments using a perfect model versus a replay buffer. The results show a clear advantage when using a perfect model, as the agent reaches a success rate of 1 more quickly and with less deviation.

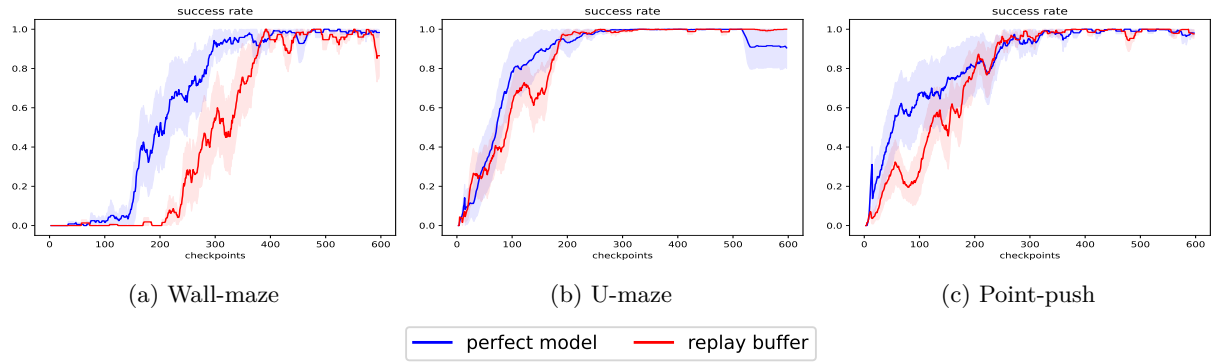

(a) Wall-maze (b) U-maze (c) Point-push

Figure 10: Comparison of ETGL-DDPG performance in navigation environments using a perfect model vs. replay buffer.

A.5 Implementation Details and Experimental Hyperparameters

Here, we describe the implementation details and hyperparameters for all methods used in this paper. All experiments were run on a system with 5 vCPU on a cluster of Intel Xeon E5-2650 v4 2.2GHz CPUs and one 2080Ti GPU. Table 2 displays the details for environments. Tables 1, 4, and 3 showcase the hyperparameters utilized in ETGL-DDPG and the baselines.

Table 1: Implementation details for ETGL-DDPG.

Hyperparameter	wall-maze	U-maze	Point-push	window-open	soccer	button-press
batch size	128			512		
number of updates per episode	20			200		
epsilon decay rate	0.9999988			0.9999992		
exploration budget N	20	40		60		
SimHash dimension	$k = 9$			$k = 16$		
soft target updates τ	10^{-2}					
discount factor γ	0.99					
warmup period	$2 * 10^5$ steps					
exploration buffer size	10^6					
exploitation buffer size	$5 * 10^4$					
actor learning rate	10^{-4}					
critic learning rate	10^{-3}					

Table 2: Environment details.

environment	$S \in$	$G \in$	$A \in$	Max steps per episode
Wall-maze	$\mathbb{R}^2$	$\mathbb{R}^2$	$[-0.95, 0.95]^2$	100
U-maze	$\mathbb{R}^6$	$\mathbb{R}^2$	$[-1, 1] * [-0.25, 0.25]$	500
Point-push	$\mathbb{R}^{11}$	$\mathbb{R}^2$	$[-1, 1] * [-0.25, 0.25]$	500
window-open	$\mathbb{R}^{39}$	$\mathbb{R}^3$	$[-1, 1]^4$	500
soccer	$\mathbb{R}^{39}$	$\mathbb{R}^3$	$[-1, 1]^4$	500
button-press	$\mathbb{R}^{39}$	$\mathbb{R}^3$	$[-1, 1]^4$	500

Table 3: Implementation details for DOIE.

Hyperparameter	wall-maze	U-maze	Point-push	window-open	soccer	button-press
batch size	256					
number of updates per episode	100					
replay buffer size	$5 * 10^5$					
actor learning rate	10^{-4}					
critic learning rate	$5 * 10^{-3}$					
discount factor γ	0.99					
action scaling	0.01					
environment scaling	0.1 for each dimension					
knownness mapping type	polynomial					

Table 4: Implementation details for SAC, TD3, and DDPG.

Hyperparameter	wall-maze	U-maze	Point-push	window-open	soccer	button-press
batch size	128			512		
update frequency per step	12			2		
action noise	$\sim N(0, 0.2)$	$\sim N(0, (0.3, 0.05))$		$\sim N(0, (0.15))$		
warmup period	$2 * 10^5$ steps					
replay buffer size	10^6					
learning rate	$3 * 10^{-4}$					
soft target updates τ	$5 * 10^{-3}$					
discount factor γ	0.99					

A.6 ETGL-DDPG Algorithm

In this section, we introduce ETGL-DDPG, as detailed in Algorithm 3, which is organized into three primary functions: `train`, `run_episode`, and `update`. The `train` function is called once at the start of the training process. For each training episode, the `run_episode` function is invoked to perform a training episode within the environment, followed by the `update` function to adjust the networks based on the experience gained from the episode.

A.7 Analyzing the Impact of N on ϵt-greedy and ϵz-greedy Exploration

The tree budget N upper bounds the option length of ϵt-greedy due to the fact that the longest path between nodes in the tree is shorter or equal to the number of nodes in the tree. This is analogous to the

Table 5: Analysis of the impact of budget N on the environment coverage.

budget N	ϵz-greedy			ϵt-greedy		
	Wall-maze	U-maze	Point-push	Wall-maze	U-maze	Point-push
5	0.36	0.55	0.36	0.76	0.94	0.40
10	**0.38**	0.91	0.38	0.97	0.91	0.41
15	0.34	0.85	0.39	0.65	0.94	0.42
20	0.30	0.84	0.40	0.83	0.94	0.48
25	0.28	**0.86**	0.40	**1**	0.95	0.47
30	0.27	0.83	0.39	1	**0.97**	0.51
35	0.25	0.82	0.40	1	0.95	0.53
40	0.24	0.82	0.40	1	0.97	0.55
45	0.22	0.85	**0.41**	1	0.96	0.64
50	0.22	0.79	0.40	1	0.97	**0.73**

role of N in ϵz-greedy, where a uniform distribution $z(n) = \mathbb{1}_{n \leq N}/N$ is used. To evaluate both methods, we assess environment coverage under varying budget sizes, calculating the coverage after 1 million training frames. Table 5 shows the results: ϵt-greedy consistently achieves greater coverage than ϵz-greedy across all environments and budget sizes. Additionally, ϵt-greedy demonstrates improved coverage as the budget increases. In contrast, increasing the budget for ϵz-greedy does not consistently improve coverage and can even decrease it in some cases. This highlights the advantages of directed exploration over undirected methods, particularly in complex environments with numerous obstacles, such as Wall-maze.

A.8 Terminal States Distribution

We analyze the order in which the agent visits different parts of the environment by examining the distribution of the last states in the episodes. To make it more visually appealing and easy to interpret, we only sample some of the episodes. The results for Wall-maze, U-maze, and Point-push can be found in Figures 11, 12, and 13, respectively. In Wall-maze, only ϵt-greedy and DOIE can effectively navigate to different regions of the environment and ultimately reach the goal area. Other methods often get trapped in one of the local optima and are unable to reach the goal. The reason some methods, such as TD3, have fewer points is that the agent spends a lot of time revisiting congested areas instead of exploring new ones. In U-maze, most methods can explore the majority of the environment. However, during the final stages of training, methods such as DDPG, SAC, and DDPG + intrinsic motivation have lower success rates and may end up in locations other than the goal areas. In Point-push, ϵt-greedy, ϵz-greedy, and DOIE first visit the lower section of the environment in the early stages. After that, they push aside the movable box and proceed to the upper section to visit the goal area. For the other methods, the pattern is almost the same, with occasional visits to the lower section.

Algorithm 3 ETGL-DDPG

Randomly initialize critic network $Q(s, a, g|\theta^Q)$ and actor $\mu(s, g|\theta^\mu)$ with weights θ^Q and θ^μ
Initialize target networks Q' and μ' with weights $\theta^{Q'} \leftarrow \theta^Q$, $\theta^{\mu'} \leftarrow \theta^\mu$
Initialize replay buffers D_β, D_e, hash function ϕ, exploration budget N

function train(Q, μ, ϕ)
  for episodes=1,M **do**
    Receive initial observation state s_1 and goal g
    run_episode(s_1, g)
    update(*success*)
  end for
end function

function run_episode(s, g)
  $success \leftarrow false$, $l \leftarrow 0$
  while t $\leq$ T **and not**(*success*) **do**
    if l==0 **then**
      if random()$< \epsilon$ **then**
        Exploratory option $w \leftarrow$ **generate_option**(s, ϕ, N)
        Assign action : $a_t \leftarrow w$
        $l \leftarrow$ length(w)
      else
        Greedy action : $a_t \leftarrow \mu(s_t, g|\theta^\mu)$
      end if
    else
      Assign action : $a_t \leftarrow w$
      $l \leftarrow l - 1$
    end if
    Execute action a_t and observe reward r_t and next state s_{t+1}
    if is_goal(s_{t+1}) **then**
      $success \leftarrow true$
    end if
  end while
end function

function update(*success*)

$$R = \begin{cases} r_t & success \\ 0 & o.w \end{cases} \qquad bootstrap = \begin{cases} 0 & success \\ 1 & o.w \end{cases}$$

  for $i \in \{t-1, ..., t_{start}\}$ **do**
    $R \leftarrow r_i + \gamma R$
    if *success* **then**
      store transition $(s_i, g, a_i, R, s_t, bootstrap)$ in D_β, D_e
    else
      store transition $(s_i, g, a_i, R, s_t, bootstrap)$ in D_β
    end if
  end for
  Sample C random mini-batches of k transitions $(s_j, g_j, a_j, r_j, s_{j+1}, bootstrap_j)$ by τ_β and τ_e ratios from D_β and D_e
  set $y_j = r_j + bootstrap_j * \gamma Q'(s_{j+1}, g_j, \mu'(s_{j+1}, g_j|\theta^{\mu'})|\theta^{Q'})$
  update critic by minimizing the loss: $L = \frac{1}{k}\sum_j (y_j - Q(s_j, g_j, a_j|\theta^Q))$
  update the actor: $\nabla_{\theta^\mu} J \approx \frac{1}{k}\sum_j \nabla_a Q(s, g, a|\theta^Q)|_{s=s_j, g=g_j, a=\mu(s_j, g_j)} \nabla_{\theta^\mu}\mu(s, g|\theta^\mu)|_{s_j}$
  update the target networks: $\theta^{Q'} \leftarrow \tau\theta^Q + (1-\tau)\theta^{Q'}$, $\theta^{\mu\prime} \leftarrow \tau\theta^\mu + (1-\tau)\theta^{\mu'}$
end function

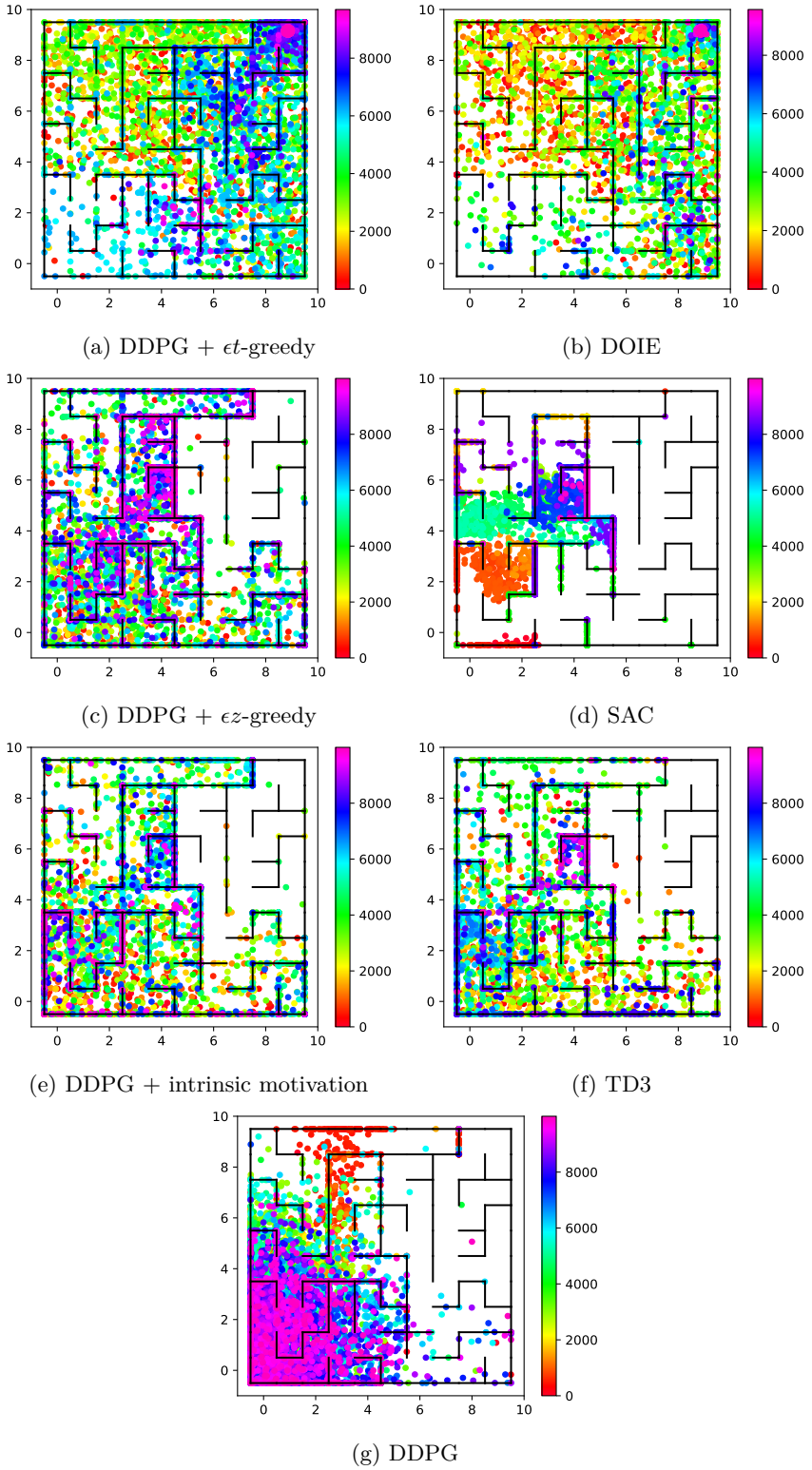

(a) DDPG + ϵt-greedy

(b) DOIE

(c) DDPG + ϵz-greedy

(d) SAC

(e) DDPG + intrinsic motivation

(f) TD3

(g) DDPG

Figure 11: The agent's location at the end of episodes throughout the training in Wall-maze.

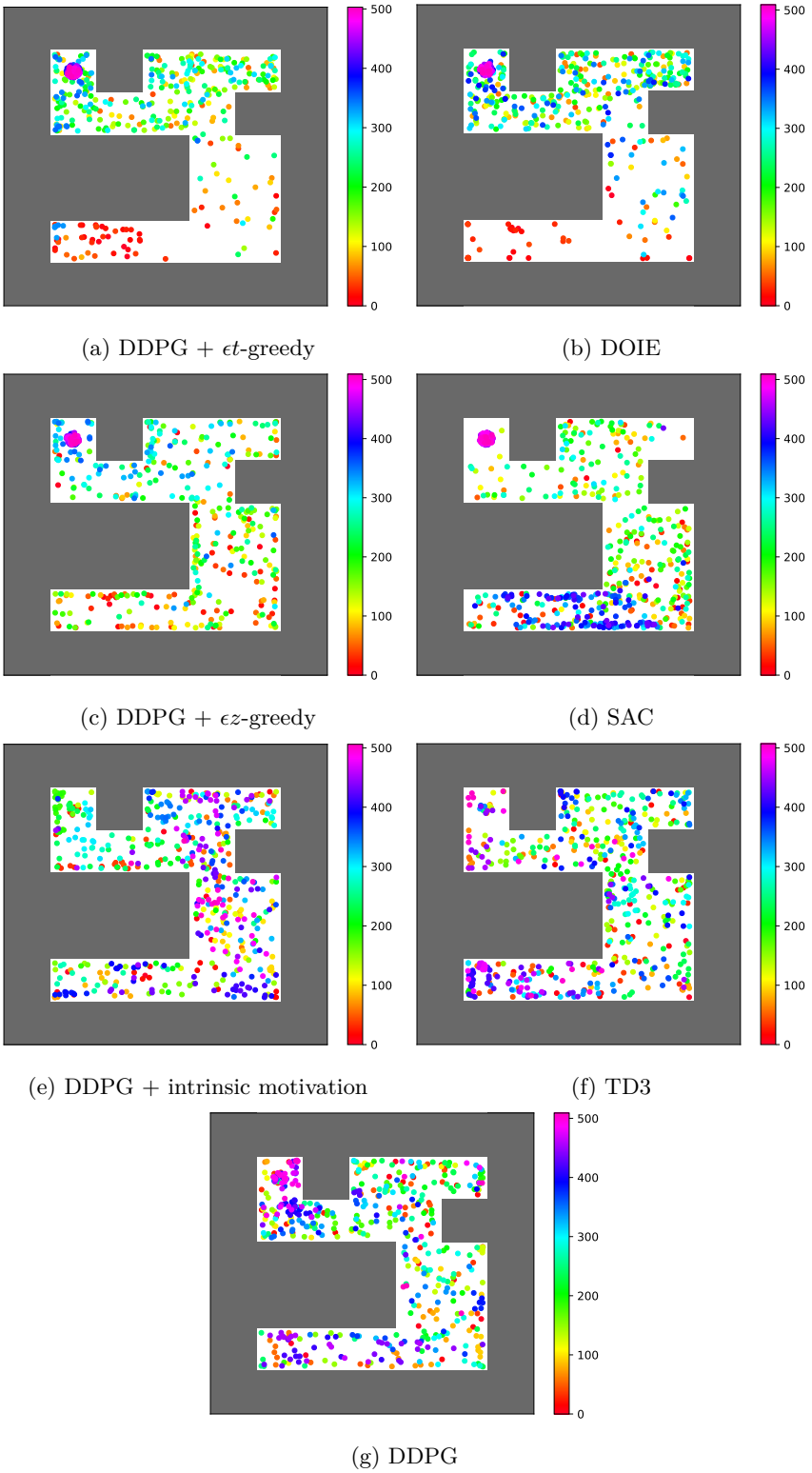

(a) DDPG + ϵt-greedy

(b) DOIE

(c) DDPG + ϵz-greedy

(d) SAC

(e) DDPG + intrinsic motivation

(f) TD3

(g) DDPG

Figure 12: The agent's location at the end of episodes throughout the training in U-maze.

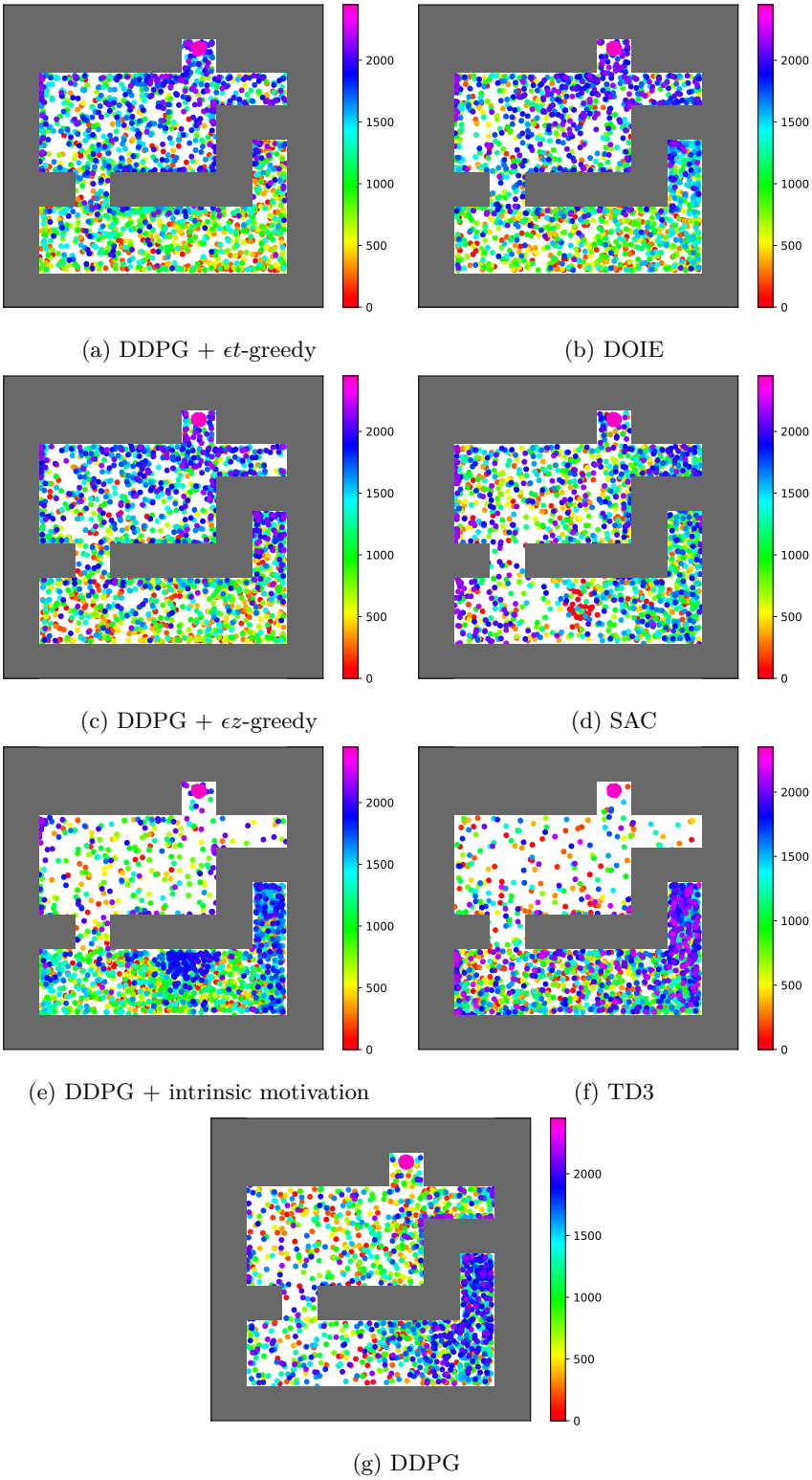

(a) DDPG + ϵt-greedy

(b) DOIE

(c) DDPG + ϵz-greedy

(d) SAC

(e) DDPG + intrinsic motivation

(f) TD3

(g) DDPG

Figure 13: The agent's location at the end of episodes throughout the training in Point-push.